UNIVERSIDAD MICHOACANA DE SAN NICOLÁS DE HIDALGO

INSTITUTO DE INVESTIGACIONES EN CIENCIAS DE LA TIERRA

NUMERICAL MODELING OF SLOPE INSTABILITY IN THE CUITZEO, MICHOACAN- REGION

T E S I S

QUE PARA OBTENER EL GRADO DE

MAESTRO EN GEOCIENCIAS Y PLANIFICACIÓN DEL TERRITORIO

PRESENTA:

ING. ÁNGEL ANDRÉS RAMÍREZ GUZMÁN

ASESOR

DR. RICARDO VÁZQUEZ ROSAS

CO-ASESOR

DR. ANTONIO POLA VILLASEÑOR

MORELIA, MICHOACÁN

FEBRERO 2019

Contents

List of figures

List of tables

Dedicatoria:

A mis padres y hermanos. Los quiero…

Agradecimientos.

Agradezco al Consejo Nacional de Ciencia y Tecnología (CONACYT) por el apoyo económico durante mi maestría.

Agradezco al Instituto de Investigaciones en Ciencias de la Tierra (INICIT) por permitirme cursar la Maestría en Geociencias y Planificación del Territorio (MGyPT), así como también a todos los profesores que participan en ella. Nada de esto sería posible sin ustedes.

Agradezco al proyecto PAPIIT (IA105016) Estratigrafía general y caracterización geológica-geomecánica de flujos ignimbríticos de la zona de Cuitzeo y su relación con la inestabilidad de taludes por brindarme su apoyo durante el transcurso de esta tesis.

Quiero agradecer a mí tutor, el Dr. Antonio Pola Villaseñor por apoyarme y guiarme de buena manera, no solo en lo relacionado a la parte técnica de este proyecto, sino también en la parte humana que debe complementar a todo estudiante de posgrado.

Doy las gracias a mi tutor interno el Dr. Ricardo Vázquez Rosas por sus muy importantes aportes al desarrollo de esta investigación. Gracias por incentivarme en momentos difíciles de la maestría.

También agradezco al M.C. Alejandro Casillas por sus aportes en el análisis de los modelos numéricos.

Agradezco mucho los consejos del Dr. Víctor Hugo Garduño Monroy y su siempre contagiante buen sentido del humor.

Un especial agradecimiento al Dr. Mario Rodríguez Martínez por brindarme un espacio para trabajar durante mi periodo de maestría. Siempre es bueno contar con personas como usted.

Hago mención también en mis agradecimientos al M.I. Pedro Martín Pacheco Valdovinos. Gracias por siempre tomarte el tiempo de compartir tus conocimientos y tu amistad conmigo. De igual manera agradezco a Víctor Hugo Méndez Bedolla por apoyarme en los exámenes de admisión y ser un buen amigo.

Agradezco a Elizabeth Correa su incondicional apoyo en todos los aspectos de mi vida.

Finalmente quiero agradecer a mis compañeros de laboratorio Guadalupe Correa, Hugo Sereno, Itzayana Torres, Carmen Alitzel y Mauricio Soto por hacer amenos los momentos difíciles. Hago mención especial de la M.C. Laura García Sánchez por su enorme apoyo en esta tesis.

Abstract:

The study of any mass movements (e.g. landslides, avalanches, debris flows, rock falls) has been a very important task for engineers, geologist and constructors since the construction of roads, dams, tunnels and open pit mines require always a slope stability analysis. The study of mass movements includes the analysis of several environment parameters and involves different science disciplines. Geomorphology, geology, climatic conditions, tectonic and the physical-mechanical characteristics of rock may be catalogued as the most important. In other words, the environment conditions (e.g. seismicity, precipitation, weathering), the temporal location of rock units and the rock genesis affect directly the geomechanical behavior of rock masses.

The southern shore of the Cuitzeo Lake is a perfect scenario were poor geomechanical characteristics of rock masses and an active extension regime has been affected the stability of slopes (e.g. normal E-W faults). A numerical simulation of an old slide that covers 2.0 km^2 and 300 m height was accomplished with the objective of understood the geomechanical behavior of rock masses that are generating instabilities in the zone as well as the main trigger factors. The study zone is mainly composed by poor welded ignimbrites and andesitic-lavas with hydrothermal alteration and the zone is mainly affected by at least three fault system. Conceptual model was accomplished based on a reconstruction of the stratigraphy in fieldwork. GSI and Generalized Hoek and Brown criterion were used for the determination of the mechanical parameters of the rock mass (ϕ; c). Finally, a numerical simulation (Plaxis 2D and GeoSlope) under four different scenarios (static, dynamic, precipitation and dynamic + precipitation) were implemented in order to determine the factor of safety and the maximum displacements for each scenario.

The stratigraphy of the slope is mainly composed by an alternation of ignimbritic units with different welded degrees and andesitic lava with high fracturing. The poor rock mass quality and the height of the slope suggest a dominant failure mechanism of general failure, similar to the soil failures. The welded degree of the different lithofacies is variable and consequently the properties of intact rock were affected. Geomechanical characterization throws values that ranges from GSI= 25-55 and mean mechanical parameters values of ϕ: 42° y c: 0.18-0.61 MPa. Factor of safety result from the numerical modeling for all the

scenarios are barely up to 1. These values decrease when a seismic acceleration in Y direction is increased up to 0.30g. This situation could be well represented in an induced seismicity analysis. Therefore, slope stability problems are controlled by poor mechanical properties of rock masses and clearly the trigger factor in the slope was seismic accelerations.

Resumen:

En el estudio de los procesos de inestabilidad de taludes y laderas en macizos rocosos intervienen una gran cantidad de parámetros del entorno que deben ser considerados. La geomorfología, la geología, el clima y la tectónica (local y regional) de la zona de estudio son algunos de los más importantes. Por otro lado, las características propias de los macizos rocosos juegan un papel de igual o mayor importancia que las características del entorno. El comportamiento geomecánico de las mazas rocosas que componen una ladera se ve afectado por distintos factores, como la génesis de la roca, la ubicación espacio-temporal de las distintas unidades de roca y en gran parte por las propiedades geomecánicas de las discontinuidades y la roca intacta.

La región sur del lago de Cuitzeo es un claro ejemplo de procesos de inestabilidad generados por un comportamiento geomecánico pobre en las unidades de roca así como una tectónica local activa en un régimen de extensión que ha generado serie de fallas normales. La zona está principalmente compuestas por depósitos ignimbríticos y flujos de lava. En esta investigación se realizó un modelo numérico de un deslizamiento antiguo que cubre un área de aproximadamente 2.0 km^2 y 200 m de altura, con el objetivo de entender el comportamiento geomecánico de las mazas rocosas que está generando las inestabilidades en la zona. Mediante trabajo de campo se reconstruyó la estratigrafía de la zona antes del deslizamiento y se utilizó el sistema GSI para caracterizar la calidad de los macizos rocosos y el criterio de rotura Generalizado de Hoek and Brown para obtener los parámetros característicos del macizo rocoso (ϕ; c) que fueron utilizados en la modelación numérica con Plaxis 2D and GeoSlope. Se analizaron cuatro escenarios distintos, en estos se incluyeron un análisis estático, dinámico, precipitación y dinámico+ precipitación.

Los resultados del trabajo de campo indican que la estratigrafía está compuesta por distintas facies de productos ignimbríticos y flujos de lava con una densidad de fracturamiento muy alta. Debido a esto, el mecanismo de falla que domina en la zona es el correspondiente a falla general, que es similar a las fallas en suelos. El grado de soldamiento de las distintas litofacies es variable y consecuentemente las propiedades geomecánicas de la roca intacta se ven afectadas. En la caracterización geomecánica mediante GSI y la utilización del criterio de rotura Generalizado de Hoek and Brown se obtuvieron valores de GSI= 25-55 y valores aproximados de de ϕ: 42° y *c*: 0.18-0.60 MPa como parámetros característicos del macizo rocoso. Los factores de seguridad obtenidos de los distintos escenarios apenas sobrepasan la unidad, estos valores solo descienden por debajo de uno cuando se considera una aceleración sísmica mayor a los 0.30g. Se concluye por lo tanto, que los procesos de inestabilidad en la zona son controlados por el fracturamiento de la zona y detonados por aceleraciones sísmicas.

1. Introduction

The study of any mass movement (e.g. landslides, avalanches, debris flows, rock falls) has been a very important task for engineers, geologist and constructors. Mass movements represent a very important hazard for populations, for example, settlements near an unstable scarp is very susceptible to be affected by a flank collapse. Otherwise, the same unstable scarp may affect important roads that communicate important cities or provoke human casualties if a big rock block hit a car or houses (Garduño-Monroy et al. 2001; Kshirsagar et al. 2016). Another important point for the study of big mass movements is the fact that we could know the evolution of geologic and tectonic processes that have been affected the morphology of the area.

In general, the study of any mass movements requires the knowledge of the geological, tectonical, morphological features of the zone and the knowledge of the physical-mechanical behavior of the material that composed the slope. Another parameter that has to be considered in the analyses of mass movements, is the environment characteristics of the area, such as the seismic susceptibility(Basahel & Mitri, 2017), weather conditions (atypical precipitation) and hydrothermal sources that weathered rock units (Fowler et al., 2018; Pola et al., 2016). In other words, the study of mass movements requires a detailed characterization of the study zone an materials that conform the slope. Particularly, this investigation presents an analysis of rock slope stability in the southern shore of the Cuitzeo Lake, this zone have been characterized for the occurrence of different slope stability (e.g. rock falls, rock-slides) phenomena that are clearly observed in affections on main and secondary roads and highways that connect very important cities (e.g. Mexico city-Guadalajara-Morelia).

The characterization of rock masses has been analyzed by the implementation of the geomechanical classifications. The most common of them, are the RMR (Bieniawski, 1973,1974,1979), the Q-system (Barton et al., 1974), and the GSI (Hoek, 1983).

These geomechanical classifications have been proved to give good results as an engineering tool, however they do not bring information about the stress-strain evolution. In this way, failure criteria were developed as a complement for geomechanical characterizations. The most used failure criteria are the Mohr-Coulomb (MC) and the Generalized Hoek & Brown (GHB) (Hoek et al., 2002), results of both are given in terms of

mechanical parameters of the rock mass: cohesion (c), friction angle (φ) and elastic modulus of the rock mass (E_m). MC criterion, proposed a linear behavior of the material, while GHB stablished a non-linear mechanical behavior. MC is often used in soil slopes and small rock slopes (<20 meters) and GHB could be applied accurately in bigger slopes (>20m). The above, highlight the importance of know the scale in which the analysis will be accomplished.

The use of GSI and failure criteria may be complemented by another studies, for example, Connors and Suárez, (2007) and (Park et al., (2016) include the use of geographic information systems (GIS) and modeling techniques for analyze the risk of collapse in an open pit mine. Agliardi and Crosta (2003) use the GSI for corroborated fracturing data and calibrate their code for the numerical simulation. Qi et al., (2016) compare different geomechanical classification for the improvement of the numerical simulations.

This investigation deals with a 300 meter height natural rock slope, it covers the study of the geologic-structural context of the study zone based on cartographic data and fieldwork. Physical-mechanical characterization of rock masses (intact rock and discontinuities) will be accomplished using the GSI for evaluate the quality of rock masses, laboratory tests on intact rock and finally, GHB will be implemented in order to obtain the mechanical parameters of the slope that permit the numerical simulation. The most used method for numerical simulations are the limit equilibrium method (LEM), which in general compare the acting forces against the resistances forces. On the other hand, the finite element method (FEM) uses iterative equations to represent the mechanical behavior of the slope and simulate the evolution of the stress-strain on the slope. Numerical simulation in this investigation were done with Plaxis 2D (www.plaxis.com) code for FEM and GeoSlope (www.geoslope.com) software for LEM. Analyzes were accomplished using different scenarios, such as seismic acceleration and the presence of water level.

1.1 Objectives

Main objective.

- Numerical modeling of slope instability on the southern part of the Cuitzeo lake, by the use of the commercial software Plaxis 2D and GeoSlope and proposing different scenarios (static, dynamic, precipitation and dynamic + precipitation).

Particular objectives.

- Construction of the geological sections of the slope by temporal, spatial and geometrical characteristics assignation of each rock unit.
- Geomechanical characterization of each single rock unit by the use of GSI and the GHB.

1.2 Study zone

The study zone is located in the central region of Mexico, specifically in the northern part of Michoacan state, along the southern shore of Cuitzeo Lake. Geologically, the area is within the large described Trans-Mexican Volcanic Belt (TMVB), into the Michoacan-Guanajuato Volcanic Field (MGVF). TMVB (Fig. 1) is an east–west, Miocene to Quaternary province (Cantagrel and Robin 1979; Nieto O. et al., 1985; Verma et al., 1985; Ferrari et al., 2000) and is the largest Neogene volcanic arc in North America with more than 1,000 km length, it covers an area of approximately 160,000 km^2. It is built on the southern edge of the North America plate, which overrides the Rivera microplate and the northern part of the Cocos plate (Ferrari et al. 2012). The geometry of the TMVB is controlled by the slab geometry, that has a 15° oblique trend relative to the Middle American Trench (Pardo and Suárez 1995; Ego and Ansan 2002). Tomography images show that Rivera plate dips at ~70° beneath the TMVB (Yang et al., 2009). It represents the last and longest continental magmatic activity: since the Jurassic, have been occurred a series of arc overlappings, which were the result of the subduction of the Farallon plate into the North-American plate (Luca Ferrari et al., 2012). The first arc was formed in Late Cretaceous to Paleogene and it consists in the prolongation of the Peninsular Range Batholiths of Baja California to the south of the TMVB in the Jalisco Block (Ortega-Rivera, 2003), the second magmatic arc is represented by granitic to dioritic plutons and basaltic to andesitic lavas exposed on the southwestern part of the TMBV.(Martini et al. 2009, 2010). On top of this rocks there are a thin layer of silicic ignimbrites, this last were emplaced in two different pulses. The first pulse affect the south of central-west part of the TMVB (Morán-Zenteno et al., 1996) while the second one is recognized in the south of the volcanic front on the central part of the TMVB (Ferrari et al., 2002; Orozco-Esquivel et al., 2009; 2010).

In turn, the MGVF, which is located in the central part of the TMVB (Fig. 1a) is delimited to the north with the Lerma river valley, while in the south is curbed by the Balsas

river depression (Kshirsagar et al., 2016), to the east, it is restrained by the Tzitio anticline (Blatter & Hammersley, 2010) and its west boundary is made by the Mazamitla volcanic gap (Kshirsagar, Siebe, Guilbaud, Salinas, & Layer, 2015). The MGVF is composed by different volcanic structures as cinder cones, stratovolcanoes, maars and lava domes. According to some authors (e.g. Hasenaka and Carmichael, 1985(Kshirsagar et al., 2016) the MGVF covers an area of approximately 40000 km^2 and comprises the largest concentration of monogenetic volcanoes in the world. Connor, (1987) carried out a study in which describes the structural geology of the MGVF, he analyzed the distribution and alignments of volcanoes and faults on a 300 km^2 area around the Paricutin volcano, finding that the volcanoes are mostly concentrated on the south-central portion. On other hand, same author found that the stratovolcanoes are concentrated into the northern part. This fact could be related to different factors or a combination of them (e.g. geometry of the subducted plate, changes in the structure of the overlying plate). In addition, the crustal configuration of the MGVF is defined by a complex faults zones arraignments (Garduño-Monroy et al. 2009; Guilbaud et al. 2011; 2012) which have been formed the Cuitzeo Fault System in the north-eastern part of the field.

Volcanic products as Plio-Quaternary basaltic andesite, andesite, and dacite rock types dominate the MGVF and cover the underlying basement. Nevertheless, recent investigations (Gómez-Vasconcelos, Garduño-Monroy, Macías, Layer, & Benowitz, 2015) found that near the eastern limit, particularly along the southeast part of the Cuitzeo lake revealed that these Plio-Pleistocene volcanism are lying unconformably over Miocene silicic ignimbrites (14.1–22.9 Ma in age) issued from multiple caldera complexes forming the Sierra de Mil Cumbres. In turn, Alaniz-Alvarez et al. (1998) suggested that monogenetic volcanoes in the central part of the TMVB follow the roughly E–W direction of the Morelia-Acambay fault system (MAFS).

MAFS is distributed in a ~30 km wide belt where WSW–ENE to E–W extensional faults formed the lacustrine basins of Zacapu, Cuitzeo, Morelia and Acambay (Ferrari et al., 1990; Martínez-Reyes and Nieto-Samaniego 1990; Pasquarè et al. 1991) (Fig. 1b). Structural studies indicate that faulting began at the end of the Miocene with left-lateral oblique motion that later became more extensional (Ferrari et al., 1990; Suter et al., 1995b). Faults in the

northwestern part of the system (Cuitzeo Lake) affect Miocene to Pliocene volcanic sequences, whereas faults in the Morelia area, in the southern part of the system, show evidences of late Pleistocene to Holocene motion (Garduño-Monroy et al. 2001; Suter et al. 2001; Szynkaruk et al., 2004). In the study zone, this dynamic structure is represented by the three main faults system identified and measured in every single outcrop.

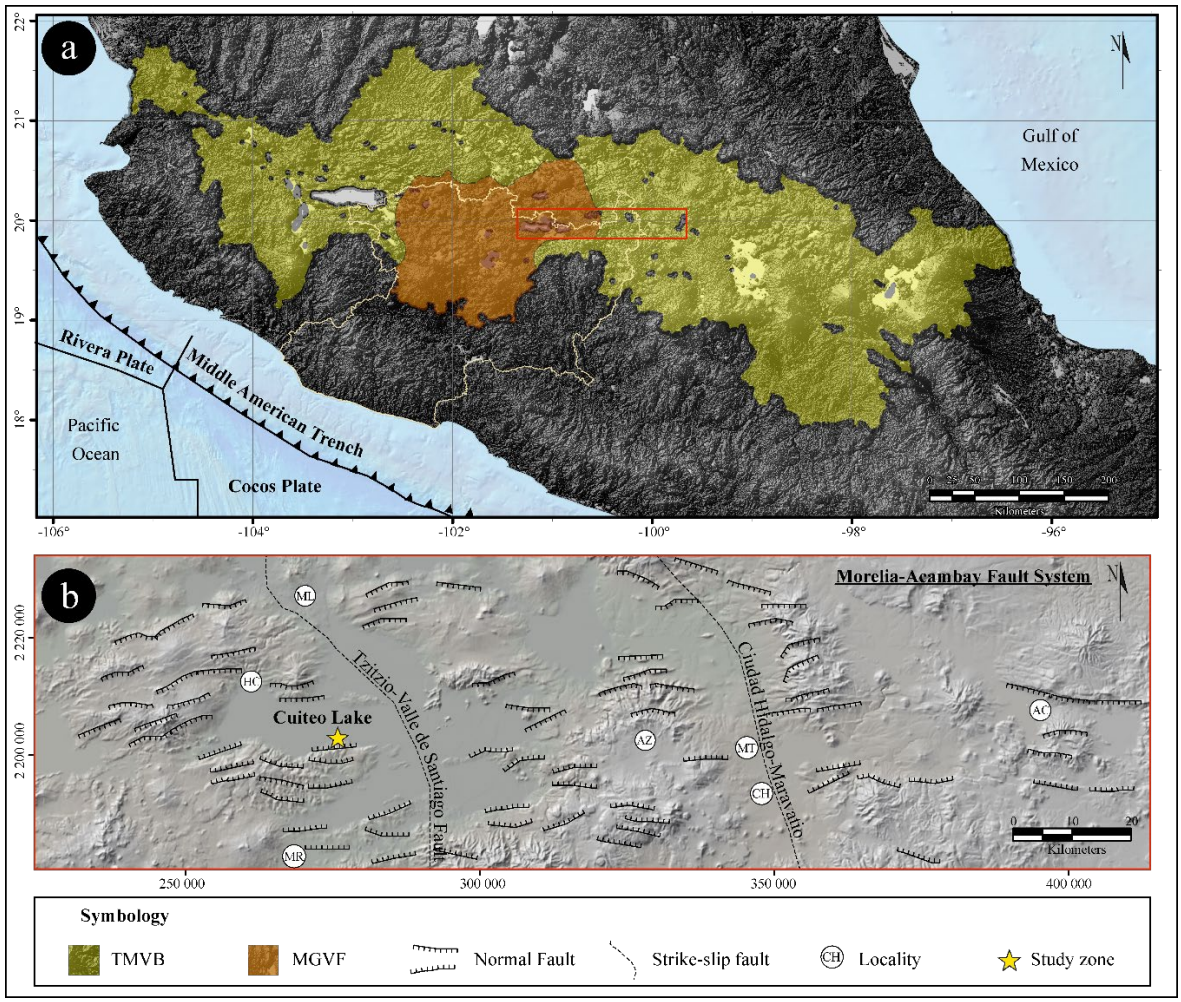

Fig. 1. a) Illustrative map of the central part of Mexico; scale of the detail: 1:250 000. b) Illustrative map of the MAFS; scale of detailed 1:20 000. Abbreviations are: HC= Huandacareo; ML= Moroleon; MR= Morelia; AZ= Los Azufres; MT= Maravatio; CH= Ciudad Hidalgo; AC= Acambay.

2. Geological-structural context

In general, the study zone is conformed by pyroclastic products and andesitic-basaltic lava, these are affected mainly by the presence of at least three regional fault systems (E-W;

NE-SW; NNE SSW). Pola et al. (2016) accomplished a geologic map, in which highlight two principal types of rock units, those are the Cuitzeo ignimbrite and the Cuitzeo andesite Fig. 2. Otherwise, Trujillo-Hernandez (2017) accomplished a more detailed geological map Fig. 3. She divided the geology in eight different sequences. 1) The granitic basement. It has been dated in 48 ma (Ferrari et al. 2012). 2) Mil cumbres sequence. It is conformed by high weathered andesitic-basaltic lavas, dated in 21.5 ma. 3) Copandaro Sequence. It is conformed mainly by the ignimbritic unit called "La yerbabuena" and "Colonia independencia". 4) Tarimbaro sequence (18.6 ma). It is composed by two different lavas, both with andesitic-basaltic composition, one of them characterized by its greenish color and the other one is characterized by a light brown color. 5) Chucandiro sequence (17.1 ma) It is composed by different pyroclastic products, which variates in color from white, light purple and pink as well as in welded degree. 6) San agustin del maiz sequence. This is conformed by lava flows, dykes and different ignimbritic lithofacies with variations in welded degree, texture, weathering (hydrothermal alteration) and lithic-pumice composition; this sequence is well described by (Nuñez-Hurtado, 2016). Also, this unit correspond to the study zone of this work. 7) Santa rita sequence (13.96-8.34 ma). It corresponds to an andesitic-basaltic dyke. 8) Monogenetic volcanoes (8.11-0.175 Ma). It is represented by different volcanic structures, most representative are: the Zapata Volcano and Chucandiro Cone. (Fig. 2)

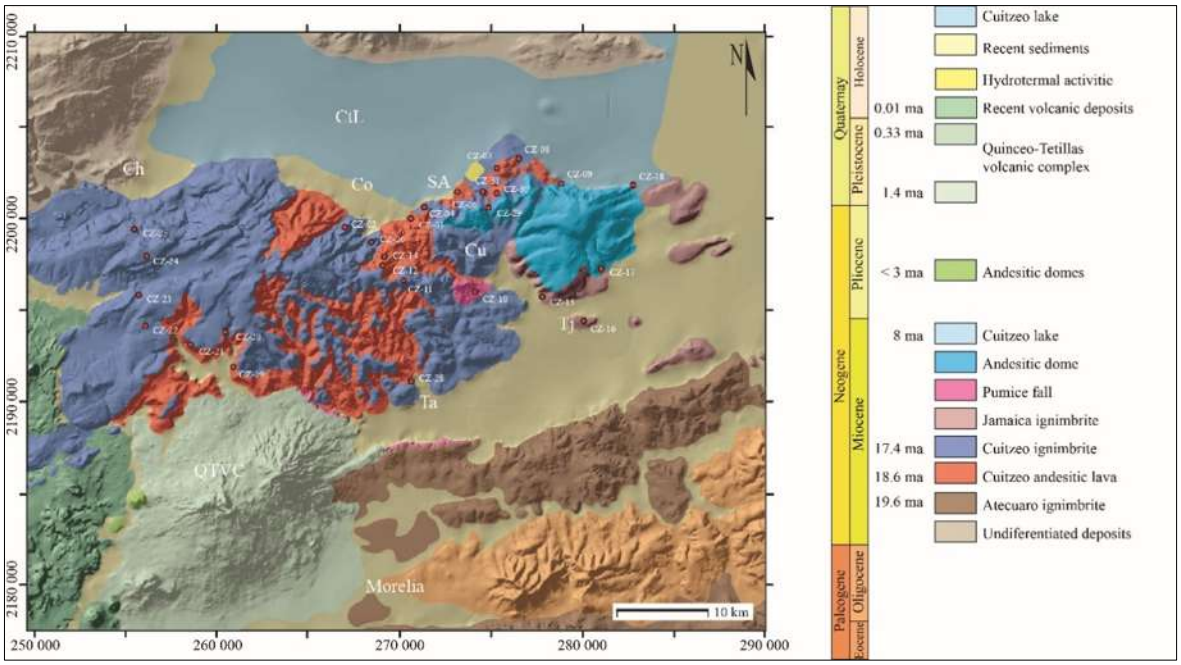

Fig. 2 General geological map of the study zone. Modified from (Pola et al., 2016)

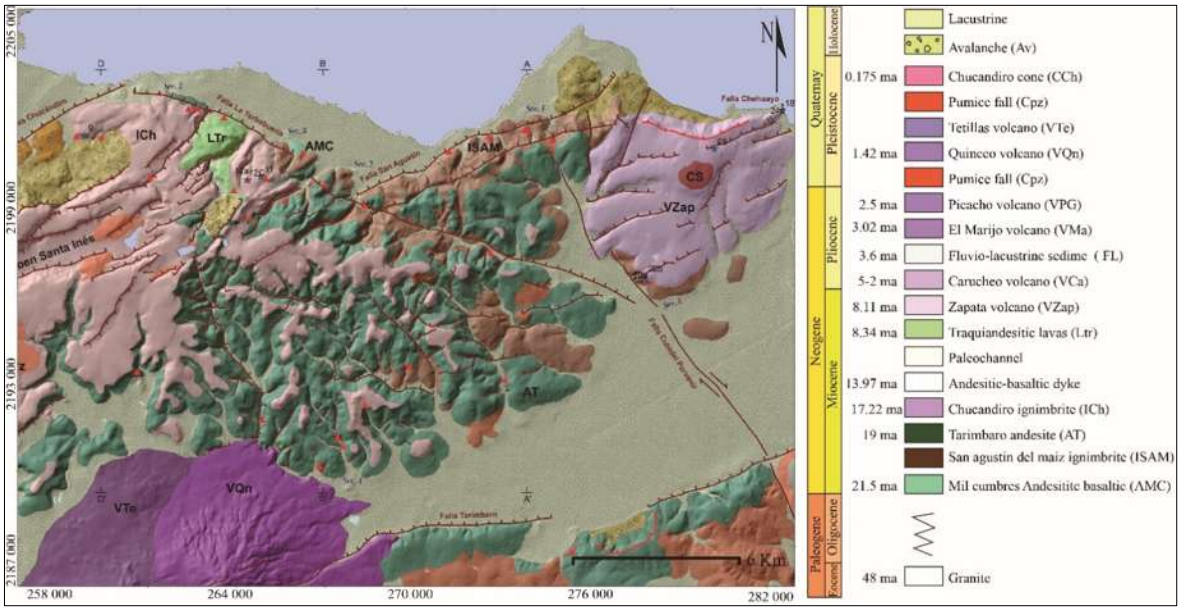

Fig. 3 Geology of the study zone. Modified from Hernandez-Trujillo (2017).

2.1 **General seismic-tectonic frame**

Seismic activity in the study zone is mainly the result of normal faults that are consequence of tectonic extension (0.2 +/- 0.05 mm / year) that affects the central part of the TMVB (Ferrari et al. al., 1991; Suter et al., 1992, 2001; Szynkaruk et al., 2004; Garduño-Monroy et al., 2009) and generated the MAFS (Fig. 1B). It is considered as seismically active (Quintero-Legorreta et al., 1988, Suter et al., 1992, Ramirez-Herrera, 1996, Suter et al., 1995b, Garduño- Monroy et al., 1997; Arduño-Monroy and Escamilla, 1996; Garduño-Monroy et al., 2001; Garcia-Palomo et al., 2000; Suter et al., 2001). Some earthquakes, reported between 1786 and 1787, caused damage in Tlalpujahua, Araro and Zinapecuaro (Urquiza, 1872, Ramírez and Reyes, 1873). Others seismic events (1912, 1979, 1998) have been located in the vicinity of Acambay and Maravatio. In particular, the 1912 earthquake partially destroyed the town of Acambay and a study of Urbina and Camacho, (1913) proves that was due a movement in the MAFS. Earthquakes on Maravatio (1979 and 1998) were due a slope failure in the Venta de Bravo fault (Astiz, 1980; UNAM, 1998). Michoacan is one of the most seismically active states in Mexico. Vazquez-Rosas et al.,(2005, 2009) makes a recompilation of historical earthquakes (since 1573) and found that exist three main sources responsible of seismicity.

3. **Background**

This chapter is a review and a compilation of the basic knowledge considerate for the well development of this investigation. It is a literature review that start with a definition of rock mass and its components (intact rock and discontinuities), as well as the most important characteristics of them (e.g. UCS, spacing, rugosity). Section 3.2 describe the most used rock mass classifications (e.g. RMR, Q-system, GSI). It is also included in this section the trigger factors of slopes (e.g. seismicity, atypical rain, overloads) and the failure mechanism (e.g. plane failure, general failure). Section 3.5 highlight the importance of the definition of the scale in the analysis and finally a brief description of the numerical modeling methods is done (FEM and LEM).

3.1 Rock Mass

Rock mass is defined as a large isotropic-heterogeneous volume of rock that is intersected by discontinuities. Rock masses is composed by intact rock and discontinuities. Intact rock is defined as the continuum portion of a rock mass that is not affected by fractures in a macroscale, in turn, discontinuities represent the discontinuous element in a rock mass (Eberhardt et al., 2004). The study of rock masses came from the necessity of engineers and geologists of know the mechanical behavior of the material in which some infrastructure works (e.g. roads, tunnel, deep foundations) are displaced.

3.1.1 Intact Rock

Intact rock refers to the unfractured blocks between discontinuities in a rock mass. The size and shape of this block is stretched related with the geometric characteristics of discontinuities (e.g. spacing, rugosity) and block size may range in size from millimeters to some meters (Evert Hoek, 1983). The mechanical behavior of intact rock is long influenced by the inherited physical characteristic of the genesis of each deposit. It is important to consider that physical characteristics of rocks may be modified by weathering or alteration. In particular, hydrothermal alteration contribute to increases in porosity and consequently the reduction of the strength. (Zhang, 2006; Pola et al., 2016).Geological classifications of intact rocks usually have a genetic basis and they may provide little information relating to the engineering behavior of the intact rock (Zhang, 2006). Some authors (Brown, 2008; Hoek & Marinos, 2005; Marinos & Hoek, 2001) and international standards in the area (CGS, 1985; ISRM, 2009) have been related the different types of intact rock with their engineering characteristics. Other authors (Kahraman, 2014; Pola et al., 2016; Schön, 2015) have investigated how the variation of physical properties such as porosity (η), density (ρ), P and S wave velocity (υ_p, υ_s) could modify the mechanical behavior of intact rock (Fig. 4).

The stress-strain behavior of intact rock could be measure with the Uniaxial Compressive Strength (UCS) and the results of this are represented in graphics stress-strain (Stress-Strain curve) in which we are able to notice not only the evolution of the mechanical behavior (e.g. *Young modulus E*) of the intact rock but also the maximum strength to axial stress (σ_{ci}). It is common to estimate the UCS by indirect tests, such as the point load compressive strength (PLCS). PLCS must be applied carefully as long as there are several

relations that not always are useful for the type of intact rock in our study. Other mechanical tests on intact rock are the Tri-axial Compressive Strength (TCS) and the Direct Shear Strength Test (DSST). These tests are very useful to obtain the characteristic parameters of intact rock such as the Cohesion (*c*), Friction Angle (ϕ) and even the Poisson Ratio (υ) with the correct instrumentation (local strain gauges) that is an essential parameter used in the numerical modelling.

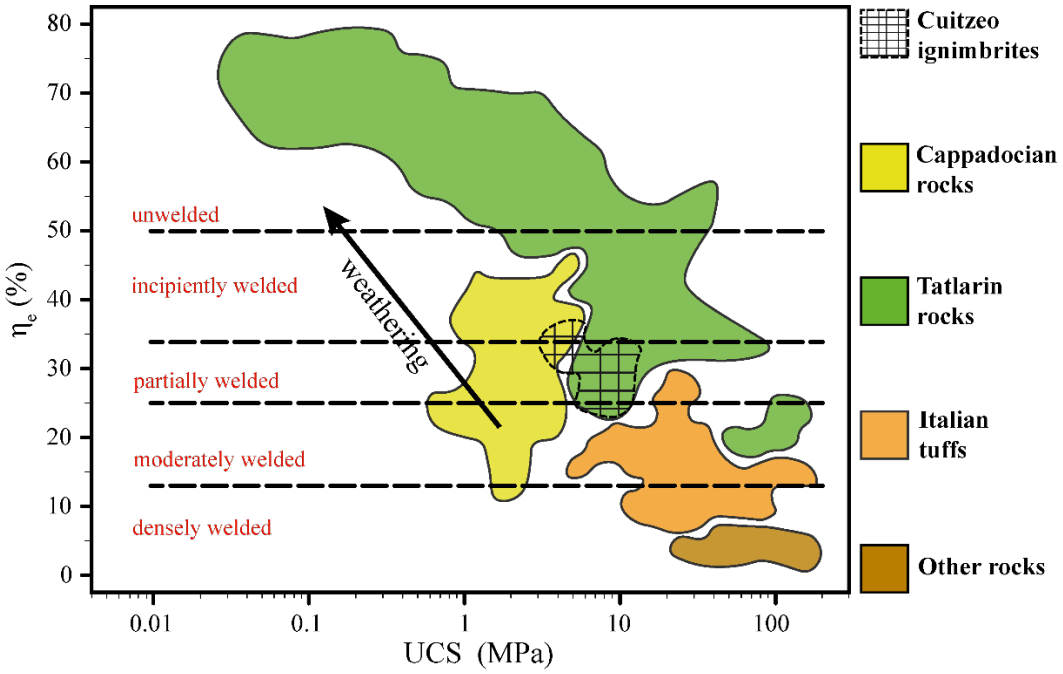

Fig. 4 Comparison of different rocks in accordance with their UCS and the effectiveness porosity (η_e). Modify from (Pola et al., 2016).

3.1.2 **Discontinuities**

The term discontinuity is use to denote any separation in a rock mass. Discontinuity is the term used to denote any break in a rock mass that have low tensile strength. Most of the time, the behavior of the entire rock mass depends on the characteristics of discontinuities, due this, an exhaustive and careful characterization of discontinuities must be done carefully Palmström, (2001). Some authors (Blyth & Freitas, 1984; Hills, 1972; Hobbs, Means, & Williams, 1976; Price, 2016; Priest, 1993) have defined different types of discontinuities from an engineering point of view. Some of them are described as follows:

Fault. It is a fracture along which there has been recognizable displacement in both sides of the plane fault. The adjacent ground to the fault is always disturbed and composed of weak material such as clay, cemented material or rock flour (gouge, breccia, cataclasite), and associated discontinuities around the fault plane. The width of fault planes could variate from millimeter to hundreds of meters.

Geologic contacts. These represent the course of deposition of different rock units. Geologic contacts are characterized for present a long persistent (tens of meters). These discontinuities may present variation in grain size, mineral composition and the cohesion between the bed-planes is enough for not consider it frictional. It is important to recognize the type of contact between different units (e.g. bedding plane, angular unconformity, disconformity pedologic contact, intrusive contact) (Crombie Howe, 1997).

Joints. In the field of geotechnics, joints are the most significant break of geological origin. The difference between joints and fault is that joints does not have a visible displacement. Planes of joints with similar values of orientation and dip may be grouped in joint sets that are usually used in kinematics analyses to predict the failure mechanism in rock masses.

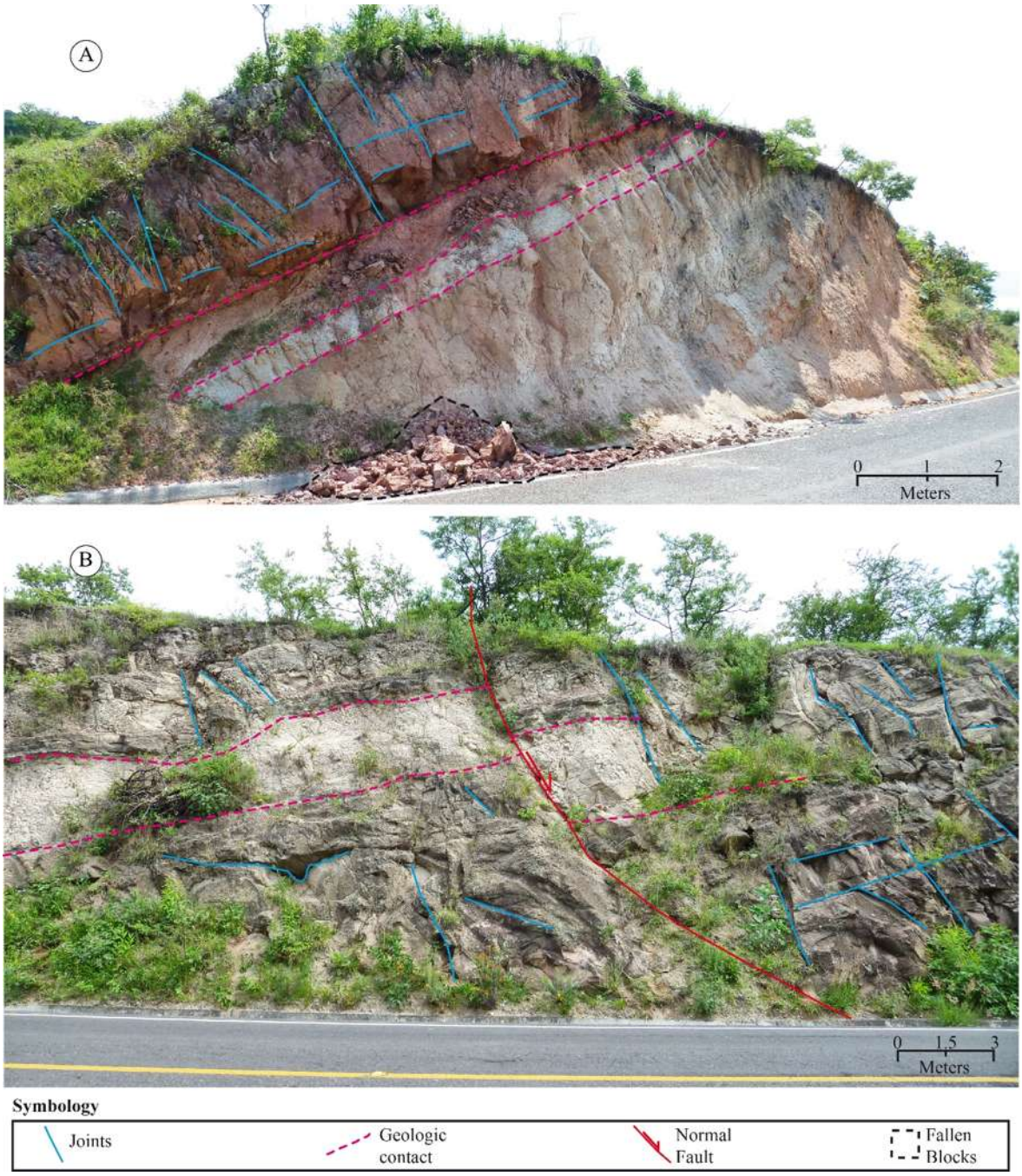

Fig. 5 A) Geologic contact between andesitic lavas and ignimbrite. Jointed rock were the fallen blocks are appreciable. B) Normal Fault and associated fractures.

International standards such as ISRM, (1978) defined ten parameters to identify the most relevant characteristics of the discontinuities that affect the behavior of rock masses such as orientation, spacing, persistence, roughness, wall strength, aperture, filling, seepage, number of sets and block size.

a) Orientation. Geometrical disposition in the space of discontinuities. It is measure in terms of the declination of the plane respect to a horizontal plane (dip) and the geographical direction of this (dip direction).
b) Spacing. It is the perpendicular distance between two discontinuities of the same joint set.
c) Persistence. It is refer to the length of discontinuity and it could end in another discontinuities, on the intact rock or out of the rock mass.
d) Roughness. Rugosity and waviness of the surface of discontinuities, this parameter define the shear strength of discontinuities.
e) Wall strength: It is the compression strength of the adjacent rock walls of a discontinuity.
f) Aperture. Refers to the perpendicular distance between adjacent rock walls.
g) Filling. The presence of material between the adjacent rock walls. Usually, this filling material is weaker than the intact rock due alteration and degradation.
h) Seepage. The presence of water flow in discontinuities.
i) Joint sets. The number of discontinuities with the same or closer orientation that are repeated along the complete rock mass.
j) Block size. Refers to the dimensions of rock blocks that are the result of the intersection of discontinuities.

3.2 Rock mass classifications

In general, rock mass classifications were created for the assignation of geomechanical properties to a rock masses involved in the construction of civil works. The first record of the development of rock mass classifications date more than 100 years ago (Ritter, 1879) and it were used to determine the support requirements for tunnel designing. Nowadays, rock mass classifications are used for different porpoise (e.g. mining, slope natural or man-made, tunnels) by engineers and geologist to determine the geomechanical characteristics of rock mases, such as the friction angle (ϕ) and cohesion (c). The geomechanical classifications integrate the physical and mechanical characteristics of both intact rock and discontinuities and are useful to characterize an anisotropic and heterogeneous media. Edelbro (2003) define rock mass classifications as the combination of different features of rock masses into different classes following a specific system.

In general, the parameters considerate in the rock mass classifications are related with the physical properties of discontinuities (e.g. joint sets, roughness, filling) and with the strength of intact rock. It is important to recognize that rock mass classifications are limited to just establish a stability criterion in terms of bad, acceptable, good or very good. In slope stability analyses, rock mass classifications are used in combination with empirical equations called failure criterion such as the GHB (Evert Hoek, et al., 2002) and the MC criterion (Mohr O, 1900). These lasts, relate laboratory tests (e.g. UCS, TCS, Till Test) with field observation to obtain not only the characteristics parameters of the rock mass (e.g. E_m, ϕ, υ) but also the principal stresses evolution (σ_1, σ_3), that are essential in any numerical simulation of slopes.

Exist a considerable number of rock mass classifications (Table 1), some of them have been developed for general purpose and other for specific applications (e.g. slopes, tunnels, foundations). However, the most common are the Rock Mass Rating (RMR) (Bieniawski, 1973, 1979, 1993), the Q-system proposed by Barton et al., (1974) and lately the Geological Strength Index (GSI) developed for Hoek et al., (1995, 1998). For the porpoise of this investigation, the rock mass classifications that will be used are briefly described next:

3.2.1 **Geological Strength Index (GSI)**

GSI was introduced by Hoek et al., (1995) as a complement for the generalized rock failure criterion that he was developed (Hoek et al 1997). GSI estimates the strength reduction of the rock mass towards different geological situations basis on visual interpretations of rock blocks and discontinuities in the rock mass. This rock mass classifications is mainly used in rock masses with poor quality (RMR<20) and it estimates the input parameters for the calculation of the rock mass strength (Fig. 6).

Table 1. Some of the most used rock mass classifications, author(s) and the application.

Most used rock mass classifications			
Name of the classification	**Short name**	**Author**	**Application**
Rock Quality Designation	RQD	(Deere and Miller 1966)	Core logging and tunnels
Rock Structure Rating	RSR	(Wickham et al., 1972)	Tunnels
Rock Mass Rating	RMR	(Bieniawski 1974)	General
Q-system	Q-system	(Barton, Lien, and Lunde 1974)	Tunnels and large chambers
Rock Mass Strength	RMS	(Stille et al., 1982)	General
Slope Mass Rating	SMR	(Romana 1993)	Slopes
Ramamurthy and Arora Classification	RAC	(Ramamurthy and Arora 1993)	Intact and jointed rock
Geological Strength Index	GSI	(Hoek et al., 1995)	Mines, tunnel. slopes
Rock Mass Number	RMN	(Goel et al., 1996)	General
Rock Mass index	RMi	(Palmstrom, 1995)	General

Slope stability analyses is a multidisciplinary task and it requires the knowledge of different areas such as geology, tectonics, geotechnics and geomorphology. The more detailed information of the zone, the more accuracy in the results. However, the complexity of the analysis will increase proportionally to the lasts. This section addresses the factors that control the mechanical behavior of rock slopes and rock mass strength as the same as the trigger factors which change the stress state in rock masses and cause the failure. Next, the possible failure mechanism in rock masses are reviewed in accordance with kinematic analyses of discontinuities. All the previous information is required for the geomechanical characterization of rock units. The objective of the geomechanical classifications is to obtain the mechanical parameters of the rock units based on its physical and mechanical characteristics. The last section explain the effect of the scale of the analysis and its importance in slope stability analyses. This section focuses in the importance of the parameters needed for the construction of conceptual models and numerical modeling that is reviewed in Section 2.1 and 2.2 respectably.

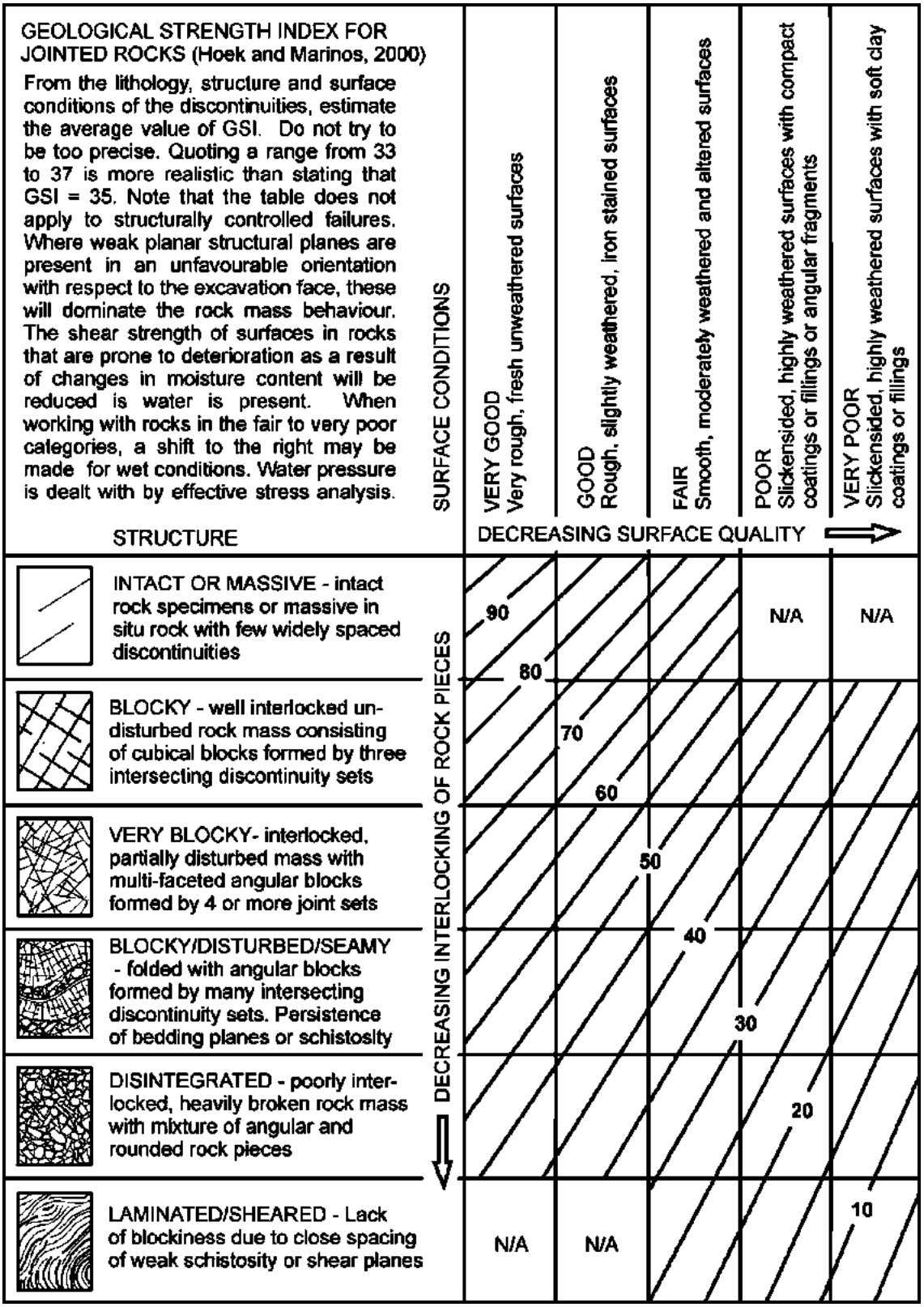

Fig. 6 GSI chart were visual interpretation is required

3.3 Controlling and trigger factors of slope failure in rock masses.

In general, slope stability analyses requires detailed information about the geology, geomorphology and geomechanical properties of each rock unit that compound the rock mass analyzed, as well as the factors that may or could cause the failure, the possible failure mechanism and the factors that influence the rock strength. In this way, it is important to make a remarkable differentiate between the internal characteristics that affect the behavior of intact rock and discontinuities and the external factors that trigger the failure. In other words, it is important to considering the evolution or modification of this mechanical behavior due to different phenomena, such as earthquakes, overloads, atypical rain etc.

The controlling factors of a slope stability analysis are defined as those that conditioning the failure without this occurs. In other words, these factors define the limit equilibrium of the slope. In this investigation, controlling factors has been grouped in four categories; morphological, geological, structural and geomechanical factors. The morphological factors are defined as the geometric and geographical positioning of the slope and the rock units which compound it. The geological factors as the name suggested are those that involves the different rock units in the slope. The structural patterns are given by the discontinuities and the physical characteristics of these lasts. The geomechanical features of rock masses are the most important controlling factor in a slope stability analysis. The geomechanical characteristics of the rock mass are needed to the understanding of the mechanical behavior of the rock mass. The geomechanical characteristics are obtained with the geomechanical classifications.

Triggers factors in rock masses are defined as the sudden changes resulting from the modification on the stress state, and induced by anthropogenic or natural factors (e.g. civil works, earthquakes, rain, erosion, weathering). This suddenly change is reflected in over-stresses in both, intact rock and discontinuities. Styles, D & Hons, (2015) define three main factors that may trigger slope failure: an additional load on the slope (including groundwater and dynamic loading); Change to the geometry (mining or erosion); or Internal rock mass degradation/damage.

Landslide occurred in November 4th 2007 on Grijalva River, located in Chiapas. Atypical rain was the trigger factor for the occurrence of the landslide that moves a volume

of approximately forty-eight million cubic meters of both, rock and soils. This landslide results in the obstruction of the river and a subsequently flood. A total of twenty-five human casualties was the result (Hinojosa-Corona et al., 2011).

3.4 Failure mechanism

An essential part of rock slope stability analyses is to identify the possible failure mechanism in the rock mass. Basis on geometry (dip direction, dip), roughness (ϕ) and the stereographic representation of discontinuities, different types of instability could be recognized. Stereographic analyzes had to be done carefully and always together with a detailed observation and geomechanical characterization of the complete rock mass. In accordance with this investigation, failure mechanism characteristics of the zone could be graphically represented in (Fig. 7). Next, a brief description of each failure mechanism:

Plane failure. This failure consists in a rock block that slid in a single plane and dipping out of the slope face (Fig. 7a). In general, there are four parameters that have been considered in a planar failure:

- The orientation of the sliding plane must be strike ±20° to the slope face.
- The dip of the sliding plane must be smaller than the dip of the slope face $\Psi_p < \Psi_s$
- The dip of the sliding plane must be greater than its angle of friction $\Psi_p > \phi$.
- The upper end of the sliding plane ends in a tension crack or intersects the upper of the slope.
- The sliding plane must be outcropped into the slope face.

Wedge failure. This failure occurs when two discontinuities that are striking obliquely to the slope face intersect. This intersection results in a sliding line in which is possible to measure its orientation (Fig. 7b). The general geometric conditions for a wedge failure are pointed out next:

- Two planes that intersect in a line; if we have the orientation and dip of the two planes, we will able to determine the trend (α_i) and plunge (Ψ_f) of the line of intersection.

- The plunge of the line of intersection must be smaller than the dip of the slope face $\Psi_i < \Psi_f$.
- The plunge of the line of intersection must be greater than the angle of friction of the discontinuities $\Psi_i > \phi$.
- The line of intersection must be outcropped into the slope face.

Toppling failure and rock fall. This differs from the other modes of failure in that it is not presented through a sliding surface. Toppling failure involves rotation and fall of rocks in a fixed base. As the same as in planar and wedge failures, a kinematics analyses could be performed for determine the conditions for a toppling failure. Goodman & Bray (1976) described two different types of toppling failure: Block toppling and Flexural toppling; the first of them occurs in rigid rock, when discontinuities form columns that dip steeply into the slope face and another discontinuity set with a wide spaced and orthogonal joint define the column height. This last could be related with a domino effect in which the columns from the back push forward to the blocks from ahead. Flexural toppling occurs when continuous columns of rock breaking in flexure as they bend forward, this can result in the formation of tension crack along the columns. It is important to note that toppling failure could be inferred as rock falls (Fig. 7c).

Circular failure. Rock masses not always content a well define set of discontinuities. Several times rock mass is compound of weak material which is highly weathered, closely fractured or the combination of the last. In these cases, failure occurs along a surface that approaches a circular shape (Fig. 7d). In other words, in a circular failure in rock masses, the slide surface is defined as the line of least resistance through the slope. In this way, circular failure in rock masses occurs when rock blocks are very smaller compared with the size of the slope analyzed. Hence, it is correct to say that the rock mass will tend to behave as a soil.

The determination of possible failure mechanisms is an essential step in all the slope stability analyses. Hence, acquisition and interpretation of field data must be done carefully and is always important make conceptual models that resemble the most important features of each slope analyzed.

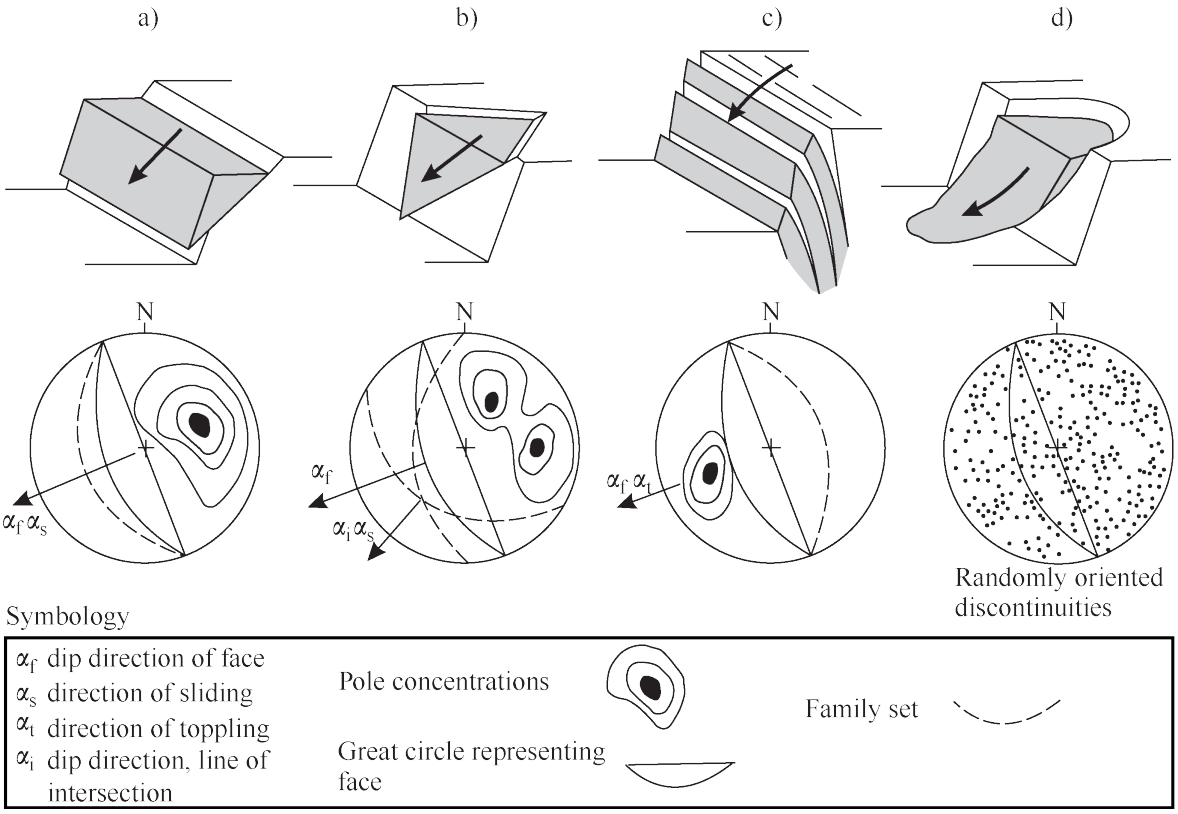

Fig. 7 Typical failure mechanism in rock and its stereographic representation. a) plane failure; b) wedge failure; c) toppling failure; d) general failure

3.5 **Effect of scale**

Many times, certain slope could be within another bigger slope. For example, when roads are constructed in mountainous zones is common to cut part of the natural slope, this cuts result in man-made slopes that are smaller in size. Due to this, the mechanical behavior and interpretation of results have to be managed carefully. Another classical example is represented in Fig. 8: a classic pit wall of 100 meters height with 3 benches. The mechanical behavior of the complete pit wall is different than in first two benches and in the first bench, as well as the failure mechanism differs. The knowledge of the scale that is been analyzed give us information about the way we confront the stability problem, as a circular failure, as a rock fall or a combination of the last two. It is interesting that we could have the three mentioned behaviors in the same rock mass (Hammah et al., 2008)

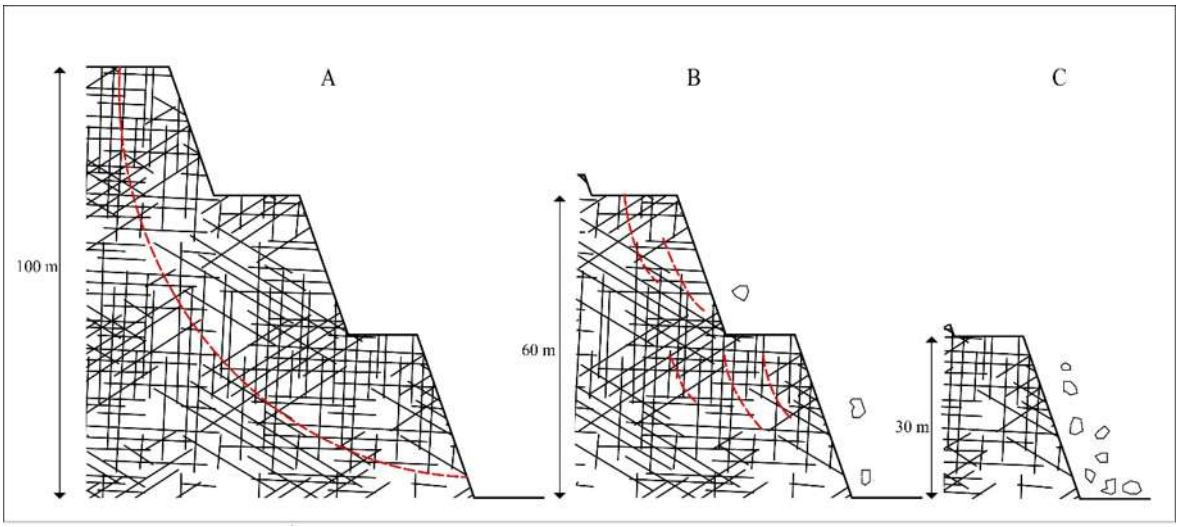

Fig. 8 Different behaviors in the same rock mass due to scale effect

3.6 **Influence of Seismicity in slope stability analysis**

Earthquakes are natural phenomena caused by the motion of geological fault on the earth crust. The motion of faults produce different waves that moves through rocks and may trigger slope failures (Fig. 9). Seismic events may affect in three ways the slopes: 1) increase the shear stress, reduction of strength due to the increase in pore pressure and deformation associated to the seismic wave. This could provoke the fail do the shear stress and even liquation in granular-saturated soils.

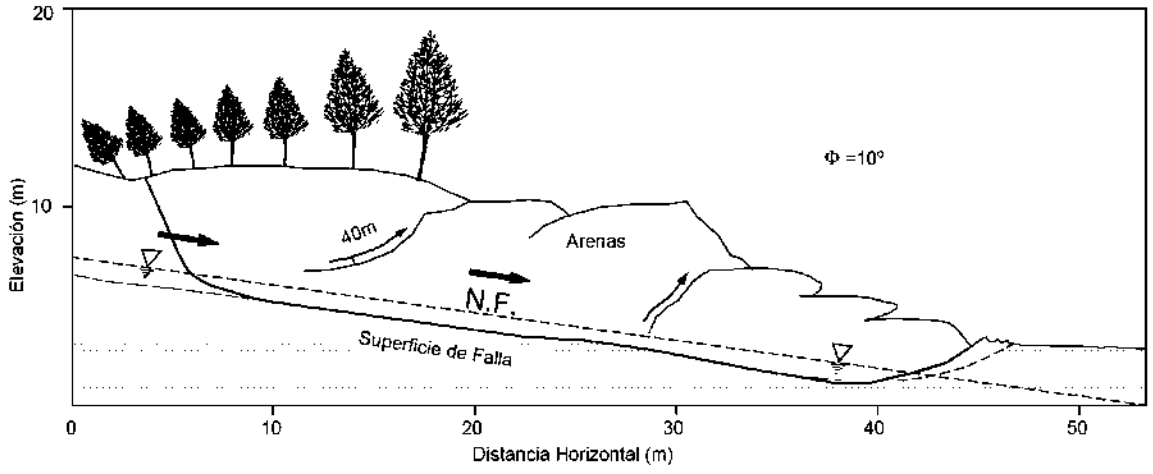

Fig. 9 Slide activated by a seismic event

Factors that has to be considered in a seismic analysis of slope stability are listed next:

-The value of the of the seismic forces that acts in the sliding mass

-The strength reduction do the vibratory loads that induce cyclic deformations. Strength reduction may reach values of 50% less in sensitive soils and the decrease could be reach 20% less during the seismic event (Makdisi and Seed,1978)

-Amplifications of the seismic force due to soft soils

-The possibility of resonance if exist the equalization between slope frequency and seismic frequency.

-Deformations in the soil mass or the liquation on sandy soils during seismic events (Seed, 1970).

The coincidence of seismic events with rainy seasons are very common in tropical areas were rainy season longs several months.

3.6.1 Peak Ground acceleration (PGA)

Horizontal PGA is the absolute value of the acceleration which is taken from an accelerogram considering its two orthogonal components. The acceleration produced by a seismic event is closely related with the motion intensity in a specific place. PGA is the most common parameter used in a seismic analysis of slopes.

Vertical acceleration have received less attention due their effect on structures and slopes is less. Generally, vertical PGA is assumed as a third part of the horizontal PGA, however, in slopes near the epicentral zones, vertical PGA gain importance and higher values should be considered. Therefore, the activation of slope failures due seismic events not only depend of the wave amplitude, but also by the frequency and the time of occurrence of the seismic event.

Seismic movements with high PGA are not necessary more destructive than those with lower PGA, this is because the time occurrence is a significant parameter for the behavior of structures and slopes (Table 2).

Other parameters for the seismic analysis of slopes are listed next:

-Peak velocity

-Peak displacement

-Wave length

-Respond spectrum

It is important to study these parameters in a Seismic Engineering book (e.g. Krammer, 1996)

Table 2 Maximum acceleration and earthquake duration (Housner. 1970)

Magnitude (M)	Duration (s)	Maximum acceleration (%g)
5	2	9
5.5	6	15
6	12	22
6.5	18	29
7	24	37
7.5	30	45
8	34	50
8.5	37	50

3.7 Conceptual models

Conceptual modeling is the previous step for any numerical simulation. The more detailed conceptual model is, the best accuracy in the numerical modeling. Conceptual modeling could be the most difficult part of the process of developing and using simulation models (Law 1991). For the last, the construction of conceptual model for slope stability analyses must be include several features such as the morphology, geometry, geology, stress field, strength of rocks, detailed characterization of discontinuities, among others. As mentioned in the previous section, the scale in where the work is developing is very important for construction of the conceptual model. The knowledge of the scale bring essential information about the importance of each features considered in the analysis.

In general the construction of conceptual model is a series of steps in which first of them involves the definition of what will be modeled and the aim of that. In other words, the beginning of any conceptual model is define the reaches and limitation of the model as the same as we have to consider that this model is only a partial description and representation

of the real world, but it has to be sufficient to address the problem situation (Robinson et al., 2011).

Taylor & Francis Group, (2011) create a summary in which propose a series of steps for an accuracy conceptual model (Fig. 9):

- Definition of the phenomena. What and how will be modeled. In this investigation a slope stability problem will be carry out.
- Determining the modeling and general project objectives. Scope and limitations of the conceptual model must be included. For example, for this investigation the principal objective of the construction of conceptual models is the numerical modeling of slope instability basis.
- Identifying the model inputs and outputs. It is essential to recognize the data we will include in the conceptual model as the same as the source of these data (e.g. laboratory tests, fieldwork, bibliography).
- Determining the model content identifying any assumptions and simplifications. It is essential always add to the conceptual model all the criteria used. In this case, the failure criteria used, the geologic contact, the characterization of discontinuities are some of the parameters must be described in the conceptual model.

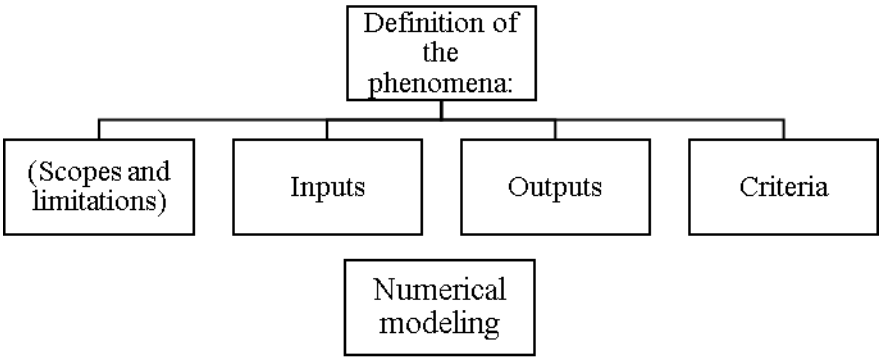

Fig. 10 Classical methodology for the construction of any conceptual model.

Several conceptual models have been constructed as a previous step for numerical modeling. Next, some of this investigation that variate since conceptual model for geothermal reservoirs to geological conceptual models are summarized:

Acocella & Puglisi, (2013) propose a conceptual model to describe and explain flank dynamics at Etna volcano in which they identify the preconditions, as due to the differential unbuttressing conditions at the volcano base, and the triggering factors, as shallow magmatic sources (dikes, reservoirs). Then, they propose five scenarios with different results if the volcano start in an unrest period. The aim of this scenarios are based on a multi-hazard analysis and consider since an edifice inflation to or seismicity on the principal fractures of the volcano. Pedrazzini et al., (2013) construct a conceptual model of the Sierre rock avalanche (Switzerland) which is one of the five largest mass movements of the entire European Alps whit an estimated volume of 1–2 km^3 (Abele, 1974). Their study was based on field observations, DEM analyzes and finally they present a numerical modeling. In their investigation, they made a comprehensive analyses of the structural and geological characteristics leading to the development of the Sierre rock-avalanche. González-Garcia & Jessell, (2016) construct a 3-D conceptual model in which he identified the geology of The Ruiz Tolima Volcanic field (RTVF) with the objective of mitigation of hazard and guide future geothermal exploration. Agliardi et al., (2001) realize a kinematic conceptual model of slope deformation on Valfurva on the eastern part of Bormio (Rhaetian Alps, Italy), they take into account the morphological, geomechanical and structural features of the zone to finally accomplished a numerical modelling to verify the hypotheses made on kinematics and driving factors of the phenomenon. They finally conclude that the importance of this deep-seated slope deformation (DSGSD) is enhanced by the occurrence of a landslide in the lower part of the slope. This last was subjected to rapid evolution and threatens the valley floor, establishing an important risk factor connected to human lives and socio-economic activities. This morphological context of the slope failure could be much related with the one we find on Cuitzeo. Brideau et al., (2009) studied famous rockslides in Europe. They construct conceptual model using detailed engineering geological mapping, rock testing, GIS data analysis, rock mass classification (GSI) and numerical modelling. The authors conclude in

the importance of considering all forms of pre-existing rock mass damage when assessing potential or operative failure mechanisms.

Another application of conceptual modeling was made by Dobson et al., (2018), he updated a conceptual model of the geothermal resource potential of the NE margins of the Tatun geothermal system (Taiwan). They analyzed existing and new fluid geochemistry data, describes new magnetotelluric data and associated 3-D modeling to incorporate these data and analyses with information from previous studies. It is important to mention this kind of studies because Cuitzeo region have been characterized lately by hydrothermal activity, probably in a short future could be necessary the implementation of studies to analyze the potential of the geothermal reservoir.

All the investigation mentioned, are stretched related with this project and the authors coincide in some characteristics that are important to take into account for an accurate conceptual model of slope instability which resemble the real conditions:

- Review of previous investigation.
- Data acquisition of Topographic maps and DEM.
- Detailed fieldwork to identify geological-structural features
- Geomechanical classifications
- Laboratory tests
- Numerical modeling

The methodology to create our conceptual model was based on the previous points and the numerical modeling is taken as another main objective due the consideration and adaptation of the conceptual model to the input model to the software.

3.8 **Numerical modelling**

All numerical modeling of slope stability problems are approximations of the physical and mechanical behavior of the rock or soil that compose the slope. The accuracy of the numerical simulation is depending basically of the assignation of geomechanical data to our conceptual model and a good selection of the input parameters to the model. In general, exists two groups of numerical analyzes: the limit equilibrium method (LEM) and the finite element

method (FEM). LEM is usually used in situation where is necessary to evaluate the stability of a lateral support systems (e.g. soil-nails, anchors) and the aim is to obtain an acceptable factor of safety (Potgieter, 2016); that is the relation between the resistance forces and the acting forces. The LEM has been used by more than 200 years (Coulomb, 1773) and has been applied in the field of geotechnical engineering, providing an accurate margin of safety against the slope failure. However, with the rapid development and improvements in computational processors, the FEM has become the principal tool in the calculation of slope stability problems. The majority of commercial codes for the analysis of slope stability are based in the FEM, software Plaxis was developed for the analysis of geotechnical problems such as slope stability, tunneling and deep excavations. This section explain some of the most used LEM as well as the basis theory of FEM. The last part is an explanation management of the code Plaxis 2D.

3.8.1 **Limit Equilibrium Method (LEM)**

After Coulomb (1773) developed the LEM for calculate the force of a fill on a retaining wall, other authors (e.g. Fellenius, (1936); Terzaghi, (1943)) have made the LEM a very useful tool for geotechnical engineers in problems of stability analyzes. In this method of analysis the principle that govern the failure mechanism is given by simple equilibrium static. In other words, all the stresses and moments are separated in those that act in favor of the failure and those that resist it. The more visible characteristic of a LEM is that the failure mechanism is proposed by the modeler, this failure mechanism can be represented by straight lines, circular arcs, log-spirals or any other slip lines (Potgieter, 2016). Exist several methods that are basis on the LEM, the majority of them are use the Mohr Coulomb Strength Criterion (MCSC) due the practicality and easy use of it in materials with a linear mechanical behavior (e.g. soil, weak rock). On the other hand, the Hoek and Brown Criterion (HBC) which stablished a nonlinear behavior of the material that compose the slope (e.g. rock masses, jointed rock).

3.8.2 **Finite Element Method (FEM)**

The FE method is a numerical technique for solving differential equations or boundary value problems in science and engineering" (Hammouri et al., 2008). The FE method has been adapted for geotechnical engineering; however there is a perception by professionals in the geotechnical industry that the FE method is too complex and there is criticism in its necessity compared to the simpler LE method considering the poor quality of materials properties often used in the analysis (Griffiths & Lane 1999). The FE method involves transferring the slopes geometry and soils properties into a mesh with a finite number of elements and nodes. Approximations are made for the continuity of displacements, the stresses between elements and the connectivity of the elements through theoretical analysis and mathematical formulations namely finite difference technique (Potts & Zdravkovic 1999; Huat & Mohammad 2006).

4. **Methodology**

The methodology was constructed according with previous works related with the numerical modeling of slope instabilities near the zone and other similar works around the world (Basahel & Mitri, 2017; Borselli, Capra, Sarocchi, & De la Cruz-Reyna, 2011; Park et al., 2016; Pedrazzini et al., 2013). First, digital terrain model (DTM) (INEGI, www.inegi.org.mx) supply were used for the construction of thematic maps such as hillshade and contour lines maps; the pixel size of DTM used was 5.0 x 5.0 meters. Two principal scarp-deposit zones were identified in the DTM and these were corroborated by a first recognition fieldwork (Fig. 12). In this way, the west scarp-deposit was choose in order to achieve a numerical simulation.

The reconstruction of the stratigraphy of the scarp was carried out by field observation. This included not only the description of the outcrops and every single rock unit, but also the collection of rock samples, the geomechanical classification of rock masses was accomplished using the GSI (Hoek et al., 1998; Marinos et al., 2007). All the laboratory tests on intact rock were implemented in the "Unidad de Petrofisica; Escuela Nacional de Estudios

Superiores-Unidad Morelia". In turn, the Generalized Hoek and Brown (GHB) criterion was used for characterized the physical and mechanical parameters of the slope, such as friction angle, cohesion, rock mass modulus and compressive strength of the rock mass. Next, seismic inversion data in the zone were used for the determination of the seismic coefficients in order to achieve a pseudo-static analysis of the slope. Also, precipitation data were collected for the inclusion of rain in the numerical simulation. Finally, safety factor (SF) of the slope were obtained by the use of Plaxis 2D, which was the best option since is possible to analyze the mechanical behavior of high-fractured and high slopes. Also, GeoSlope were used in order to verify the results in Plaxis2D.

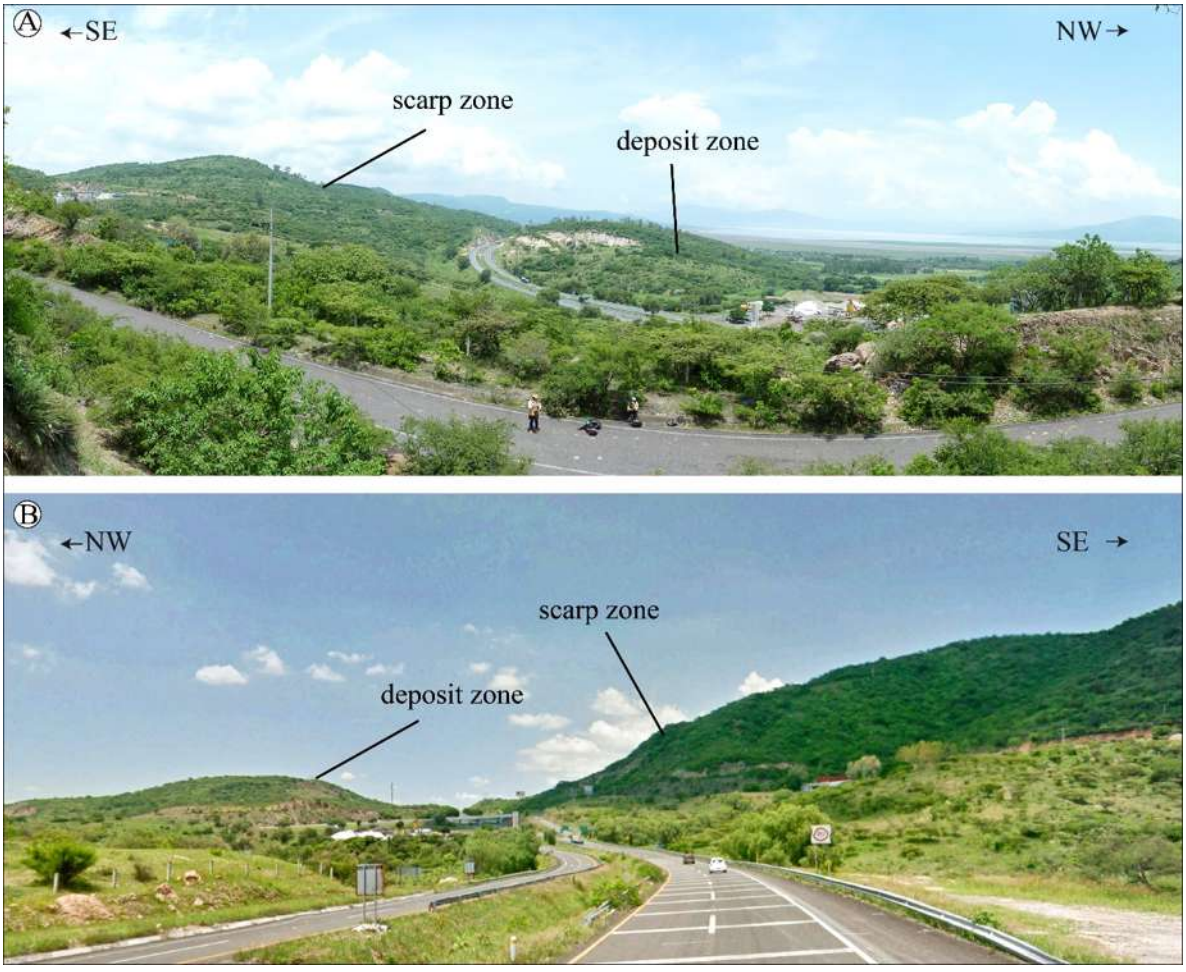

Fig. 11 general view of failed slopes.

In general, the methodology was separated in two phases: 1) construction of the conceptual model and 2) the numerical modeling. Conceptual model construction involves in long terms, the data acquisition of physical and mechanical characteristics of rock masses,

as well as the reconstruction of the geological configuration of the scarp and deposit zone. On the other hand, numerical modeling cover specific areas such as the definition of border conditions, obtaining input parameters, model calibration, as well as fitting and idealization of the conceptual model. Fig. 11 show the general diagram of methodology.

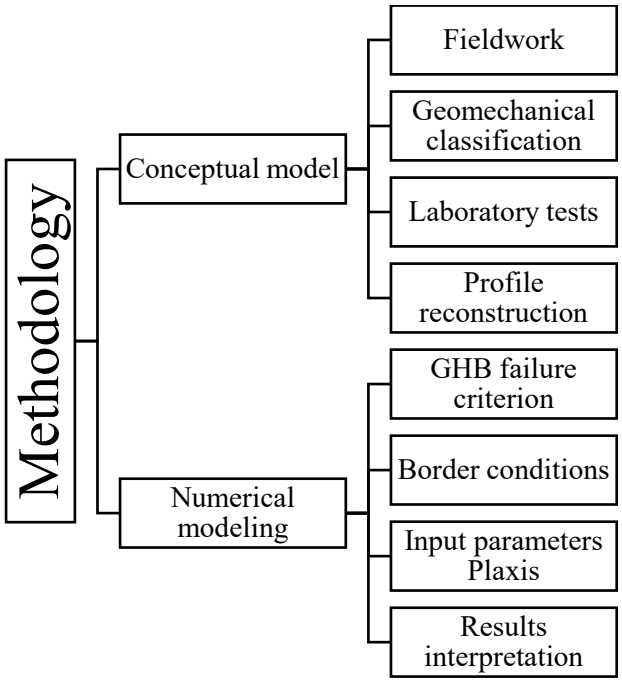

Fig. 12 General diagram of the methodology using for this investigation.

4.1. Conceptual model

This section presents the steps for the conformation of the conceptual model. It includes the activities of cartographic review, fieldwork, laboratory tests on intact rock, the idealization of the slope model and the adaptation of all conditions that best represent the real characteristics.

4.1.1 Fieldwork

Cartographic and DTM supplies (INEGI; www.inegi.org.mx) were used in the delimitation of the study zone. Detail scale of DTM used was 1:10 000 and pixel size of 5.0x5.0 meters. The scarp of the failure as well as the deposit zone were identified basis on the morphological characteristics of the area (Fig. 12) and a first recognition fieldwork.

Thirty outcrops were reviewed, both natural and anthropogenic. Fieldwork included not only the description of outcrops, but also the collection of rock samples. Outcrops were described in accordance with his color, texture, mineralogy (hand specimen). Outcrops were numbered follow with the root "Cut" that represent the city of the study zone (Cuitzeo), then it were numbered from 01 to 30 basis on the order that it were reviewed. The geographic localization of outcrops were pointed with a high precision GPS "Trimble Nomad 900G" and the elevation were corroborated with the altimeter integrated in a "Fenix 3" watch with precision of ± 1.0 meter. Collected data from fieldwork were used for the reconstruction of the stratigraphy of the scarp and de deposit zone. Profiles were constructed with the DTM in the software ArcMap ver. 10.3 (ESRI, 2016) (Fig. 13).

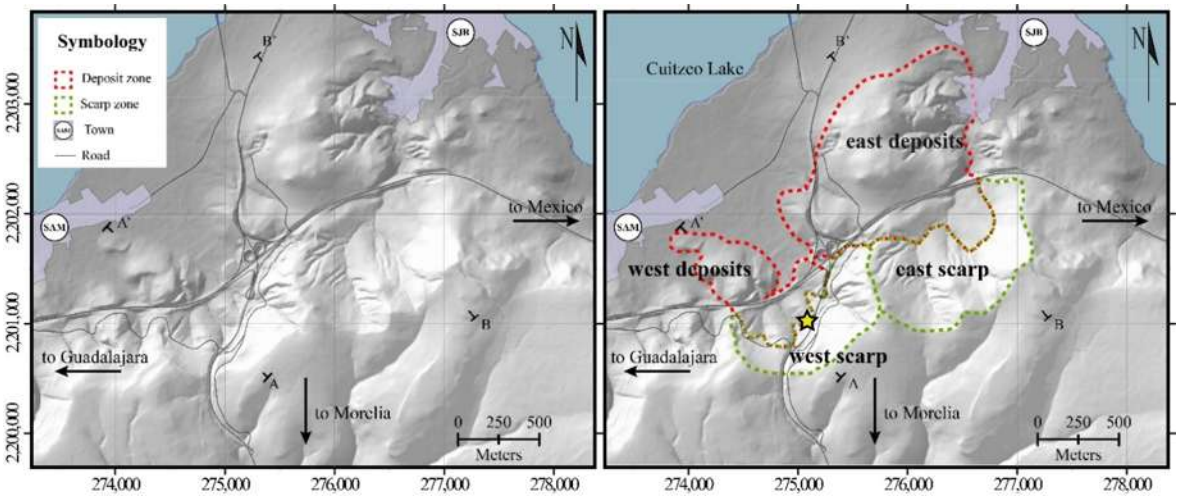

Fig. 13 Delimitation of the scarp and the deposit zone. Coordinate system UGM. Datum WGS 1984

Fieldwork included also the description of hand specimen of all the rock units that composed the scarp and de deposit zone and the sample collection for laboratory tests. A total of 10 different lithologies were described in accordance with their color, rock matrix and mineral composition which was observed with hand lens (20 x). Later, samples were collected for laboratory tests such as real and bulk density, permeability and UCS. Fig. 14 shows an example of the collected sample in field, as well as a hand specimen described.

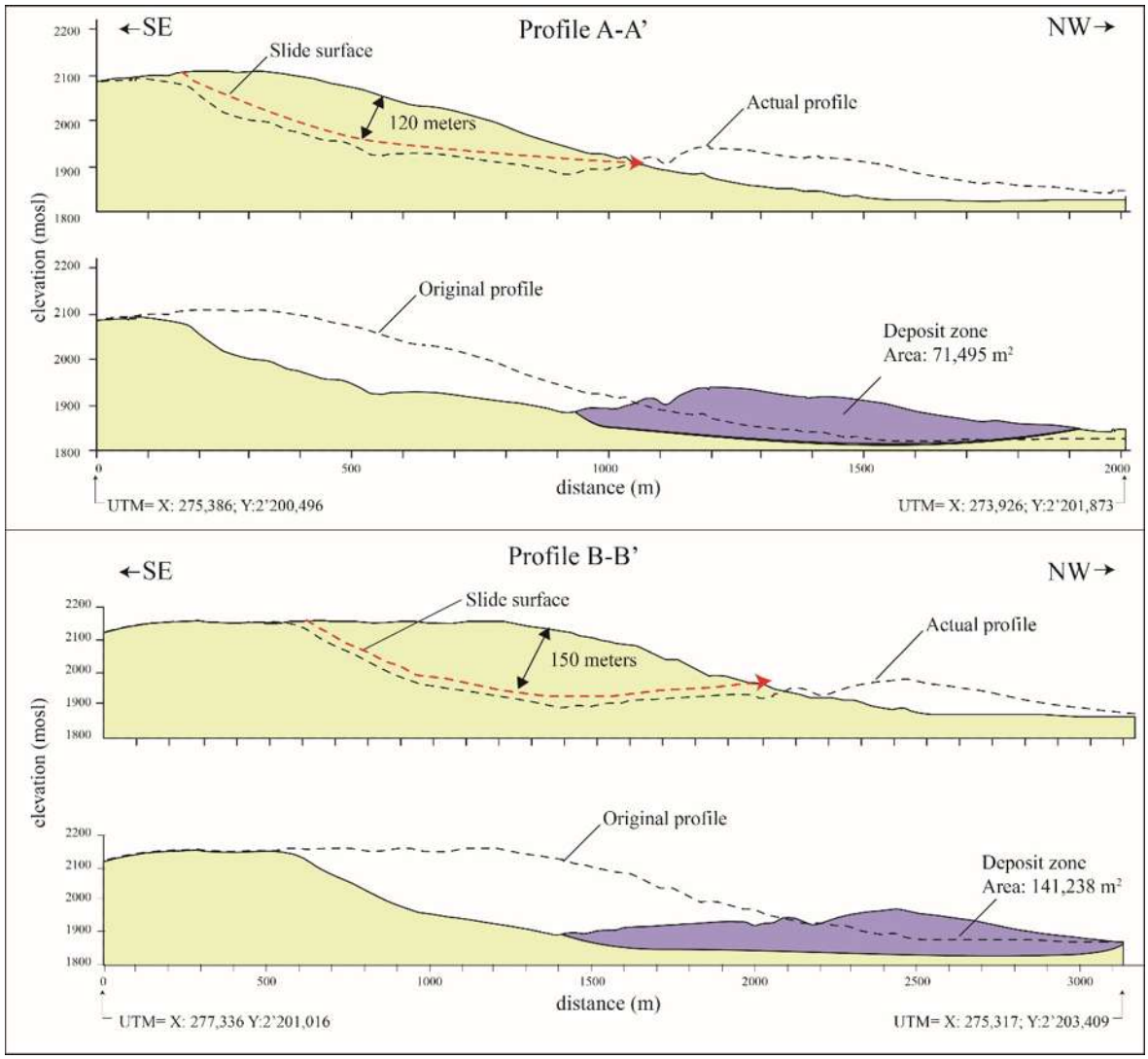

Fig. 14 Constructed profiles in ArcMap ver. 10.3 (ESRI, 2016)

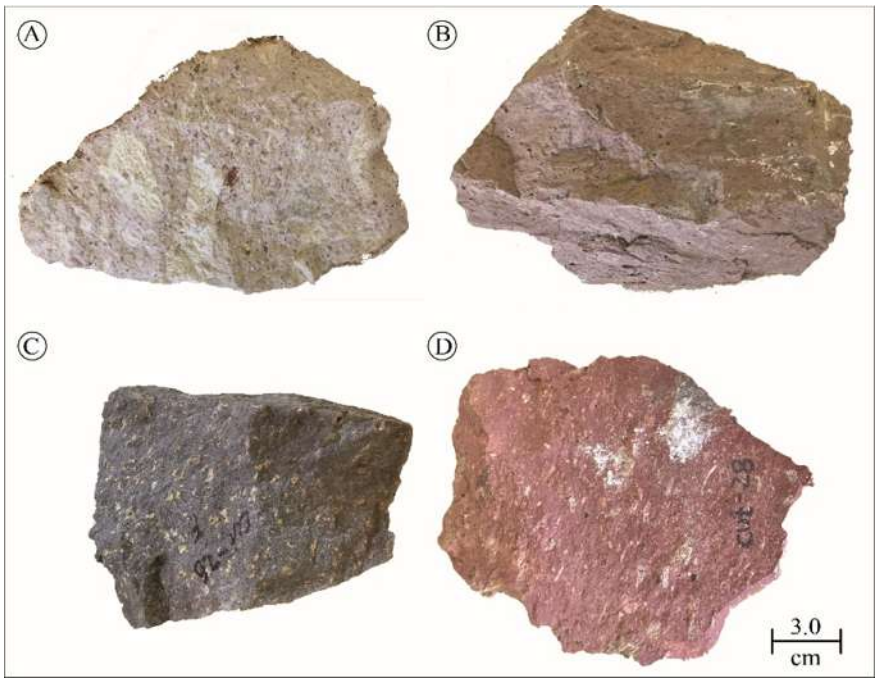

Fig. 15 Samples collected from fieldwork and hand specimen described.

4.1.2 **Laboratory tests**

Characterization of the physical and mechanical properties of intact rock were implemented in the “Unidad de Petrofisica ENES-Morelia”. In this section is presented the methodology used not only for the preparation of samples, but also the steps followed in the tests. Bulk and real density were determined using Helium picnometry technique, porosity using mercury intrusion, UCS were obtained indirectly by the PLSI and all the tests were carried out followed the stablish on ASTM norms. Eight different irregular samples were collected directly from field. Then, samples were prepared in different geometric shapes; cubic samples were used for the determination of the PLTS and bulk density. Cylindrical samples were prepared for the determination of real density and porosity.

Bulk density

Bulk density is the relation between the volume of a dry rock specimen (including the volume of pores) and its weight. Ten rock specimens were prepared in a cubic shape in order to facilitate the measure of its dimensions. Measures were took with a high precision caliper

(±0.01mm) and the average of three measures per side were took in each sample, finally were multiplied for the determination of the bulk volume of the sample. Next, all samples were dried in an electrical oven during twenty-four hours at a mean temperature of 70 °C, after that they were weighted by second time to verify that the variation was not higher than 0.03%. Weight were measured in a high precision balance (±0.0001gr).

Real Density

Real density of rock specimens is defined as the relation between the volume of solid phase and the weight. It differs from bulk density that not consider the volume occupied by pores.

Real density was determined by helium intrusion, an automatized pycnometer was used for this purpose. Samples were prepared in a cylindrical shape with radio of 25 mm and 50 mm length (Fig. 15 B).

Point Load Strength Test (PLST)

The PLST is an index test for classify rock specimens basis on their strength. The PLTS not only measure the Point Load Strength Index (I_{s50}) but also is used to predict other strength parameters such as uniaxial tensile (UTS) and compressive strength (UCS). The advantages of the use of PLST is that there is not a special procedure to prepare the specimens, thus irregular specimens could be used. In this study, PLTS have been used to indirectly obtain the Uniaxial Compressive Strength (UCS) and use it as a parameter of strength resistance of intact rock in the geomechanical classification.

The preparation and test of the specimens have been performed following the stablished on the ISRM-RTH-325-89. A total of twenty-four specimens have been analyzed (Fig. 15 A). The Point Load Strength Index (I_{s50}) was obtained as follow *(for the detailed process consult Apendix):*

First, the Uncorrected (I_s) point load Strength is calculated as:

$$I_s = \frac{P}{D_e^2} \quad (1)$$

Where D_e^2 is given by $4A/\pi$ and *A=WD=minimum cross-sectional area of a plane through the platen contact points.*

Fig. 16 Cubic samples used in the physical and mechanical characterization. A) Samples after the point load test; B) Samples before the point load test; C) Specimen of intact rock failed.

I_s varies as a function of D_e, in axial, block and irregular lump tests. Because of the last, a size correction must be applied to obtain a unique Point Load Strength value for each rock sample. This value can be use for purposes of rock strength classification. To calculate the I_{s50} including the size correction, the next formula was used.

$$I_{s50} = F \times I_s \quad (2)$$

Regularly, ISRM norms are used to correlate the PLS and UCS, nevertheless, in this investigation was used the relation (3) made by Kahraman, (2014). This relation is used since it is made particularly in pyroclastic rocks with similar physical and mechanical properties (e.g. density, porosity, PLS).

$$UCS = 2.68e^{1.93I_{s50}} \quad (3)$$

UCS was calculated for each of the twenty-four specimens and an average of the strength value was calculated discarding the higher and the lower value. The values were used in Hoek and Brown failure criterion (Bieniawski, 1973)

Porosity and Permeability

Porosity and permeability are physical properties of rocks and their study in slope stability analyses is essential. Rocks under saturated conditions changes its mechanical behavior due the presence of water into their pore system. This investigation included scenarios were not only a phreatic level is considered, but also precipitation data from meteorological stations near the zone. Porosity and permeability data were obtained in laboratory, by the use of a gas pycnometer and a gas permeameter respectably.

Porosity is defined as the fraction of the bulk volume of a rock specimen that is not occupied by the solid framework (Tiab and Donaldson, 2015). For this work, porosity was calculated according with the next statement:

$$e = \left(1 - {\rho_{bulk}}/{\rho_{real}}\right) * 100 \quad (4)$$

Where:

e= total porosity (%)

ρ_{bulk}= *bulk density of the sample (Kg/m^3)*

ρ_{real}= *real density of the rock or solid density (Kg/m^3)*

The determination of ρ_{real} and ρ_{bulk} was explained in section 4.1.2.2.

Permeability is defined as the ability of rocks to conduct fluids into its porous system (Tiab and Donaldson, 2015). Values of permeability greatly depend on connected porous (effective porosity) and the characteristics of them (shape, size, distribution) (Romaña, 2014). Permeability is given in Darcy (D) or m^2 units (1D=9.869233x10^{-13} m^2), however, permeability of rocks are low and it is very common to express permeability in a smaller unit mili-Darcy (1000mD=1D). Calculations of permeability are derived from the Darcy law on liquids under steady state and laminar flow. Mathematically, permeability is expressed in the next form:

$$k = \frac{\mu Q L}{A \Delta P} \qquad (5)$$

Where:

k: permeability (D)

μ: dynamic viscosity of the liquid (Cp)

Q: flow rate (cm^3/s)

L: length of the sample (cm)

A: transversal area of the sample (cm^2)

ΔP: pressure gradient inside the sample (atm)

Calculation of permeability for this investigation was obtained using a Gas permeameter (Nitrogen) Fig. 16. GasPerm are basis in the theory of Suárez, (2014). He stablished the next equation for determine the permeability for particular gas:

$$k_g = \frac{\mu_g \ P_b Q_b L P_{atm}}{A \Delta P P_m} \quad (6)$$

Where:

K_g: permeability to gas (D)

μ_g: gas viscosity (Cp)

P_b: atmospheric pressure (atm)

L: length of the specimen (cm)

A: cross sectional area of the cylinder (cm^2)

Q_b: atmospheric flow rate at P_b (cm/s)

P_m: mean core gas pressure (atm)

Klinkenberg discovered that permeability is less when the fluid used is a gas than when use a liquid, due that, he established a relation between gas permeability (K_g) and liquid permeability (K_L) as follows:

$$K_L = \frac{K_g}{1 + {}^{b}/_{P_m}} \quad (7)$$

Where:

K_L*= liquid permeability (real permeability)*

K_g*= gas permeability (theoretical)*

P_m*= mean pressure*

b= Klinkenberg correction factor

The tests were carried out following the stablished on the ASTM D4525-13. Five measures of K_g were accomplished, keeping constant the value of ΔP. Values were graphs on a 2 axis table were Y axis correspond to K_g and X axis is the $1/P_{mean}$ (Fig. 17)

It could be stablished that non-porous rock have zero permeability, Permeability on rocks were done in laboratory and a gas-nitrogen permeameter was used, samples used for this test were prepared according with the norm ASTM D4525-13 as well as the procedure of the test.

Fig. 17 Gas permeameter model AP-123-002-0. Maximum confining pressure of 400 psi.

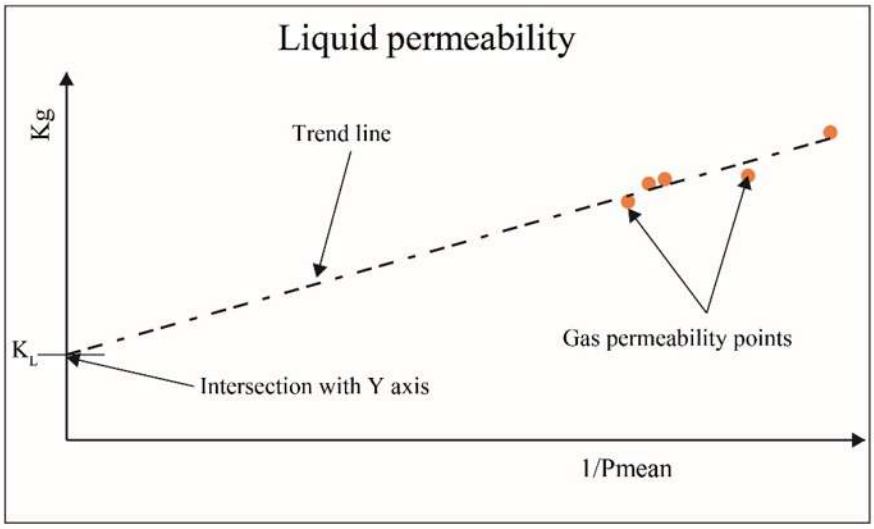

Fig. 18 Graph used for the obtention of the KL. Orange points represent one permeability test of the same specimen, dashed line represent the trend line of the five tests.

4.1.3 Slope geometry idealization

Natural slopes in difference with hand-made slopes (e.g. road cuts, foundations, deep excavations) does not have a well-defined angle respect to an horizontal plane, due this, an idealization is needed to represent the most frequent angle along the all slope. A slope model map was conducted using ArcMap v. 10.3 based on the DTM previously mentioned.

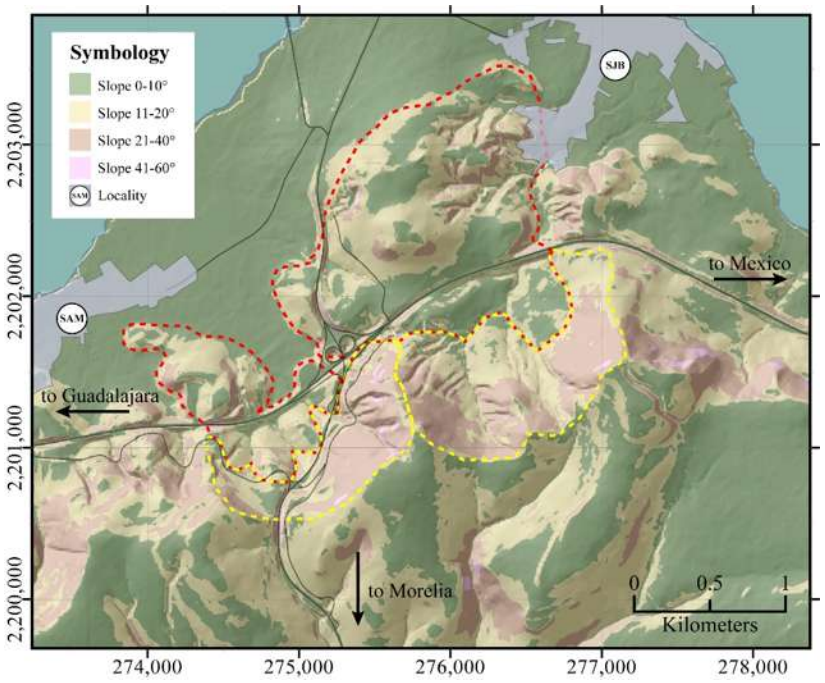

Fig. 19 Slope model of the region. Base map resolution 1:10,000. Symbology: SAM: San Agustin del Maiz; SJB: San Juan Benito Juarez.

Map was categorized in different angle ranges. From 0° to 10° the most flat zones of the study zone which cover the majority of the total area, the yellow zone correspond to angles from 11° to 20°, zone with angles between 21-20° is not the biggest, however, this zone correspond to the majority of the slopes. Due this, the angle proposed for the model was 38° which was also observed in fieldwork.

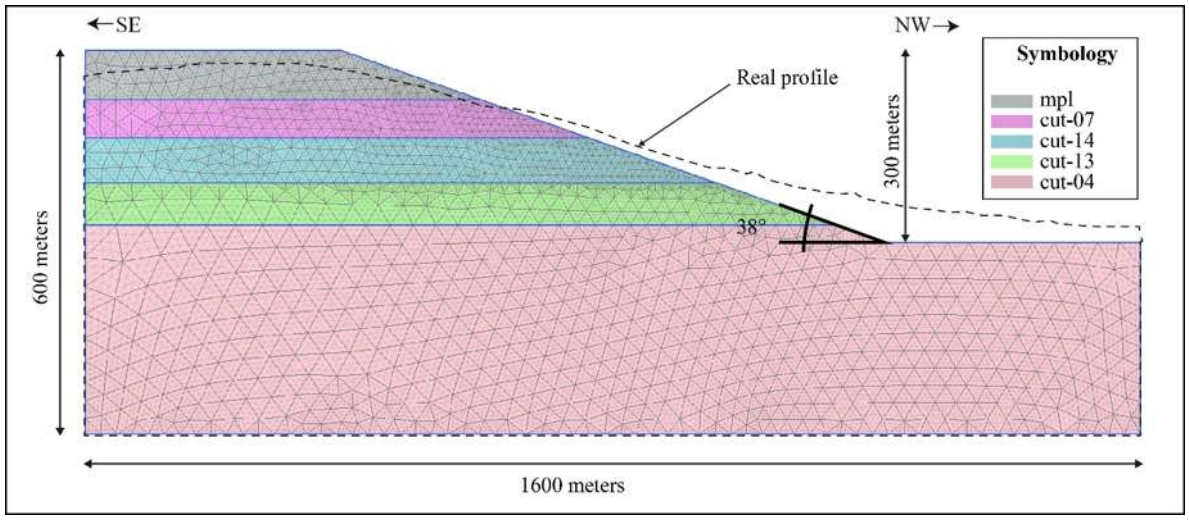

Fig. 20 proposed profile. Dashed line represent before the landslide occurrence.

4.2. Numerical modeling

Two different methods were used in this investigation in order to compare the results. FEM was accomplished with Plaxis 2D software, on the other hand, LEM was carried out with Geoslope software. This section presents the methodology used for input all the obtained parameters and the output results interpretation. Four different scenarios were simulated in order to obtain a FOS: a) static, b) pseudo-static dry c) pseudo-static + rain. It is important to highlight that software GeoSlope is assume the theory that materials behave linear-elastic, same as proposed by the MC criterion, however, the parameters calculated by the GHB (φ, c, E_m) could be used without no problem.

In general, both software (Plaxis2D and GeoSlope) were feed with the same data results from the section 4.1. Plaxis2D were selected since it is the more suitable for the simulation of non-structurally controlled failure in rock masses that are more than 30 meters

height. It is based on the FEM and it was developed for the analysis of deformation, stability and groundwater flow in geotechnical engineering. On the other hand, GeoSlope is based on the LEM and the type of analysis used was the Morgenstern-Price (MP) as long as this method differs with the other LEM (Fellenius, Bishop, Janbu) in that MP is the unique that considerate acting normal and tangential forces in each slope slice. GeoSlope was used in order to corroborate the results from the Plaxis2D. However, the operation of these softwares is very similar and could be summarized as follows:

a) Characteristics of the project:

In this parts are defined the conditions of the entire project, such as the name of the project, units (SI) and the workspace dimensions. Also in this part, are defined the quality of the mesh. For this work, the 15-noded mesh was selected by recommendations of the users manual.

b) Define the geometry

Slope geometry was simplified by the main dip of slopes in the region, which is mainly between the 20 and 40º. The height of slope was took from the DTM constructed in ArcMap ver. 10.3, finally the top-bottom and deep length of the slope model was proposed in order to these not affect the slope analysis 350 meters on each side and 300 meters deep Fig. 19

c) Define the materials

The materials were defined in accordance with the field observations, GSI, physical-mechanical characterization of the intact rock (e.g. UCS, ρ_{real}, ρ_{part}) and the use of the GHB parameters (φ, c, E_m). Nine material were created in accordance with the samples collected in fieldwork. Eight materials are pyroclastic products with different welded degrees and mineral composition, one sample was taken as representative from the andesite unit. The model was simplified into 5 representative layers, Fig. 19 shows the different units used.

d) Mesh

Mesh was created automatically by the software with a total of 2662 triangular elements and 21717 nodes Fig. 19

e) Scenarios definition

Four different scenarios were evaluates, the displacements and FOS were compared in all of them:

1) Static: just specific weight of the materials were considerate.
2) Seismic: the seismic analysis was done considering the pseudo-static acceleration from section 4.2.2
3) Precipitation: for this scenario were considered the maximum precipitations from section 4.2.3 and the phreatic level.
4) Seismic-precipitation: the combination of scenario 2 and 3

f) Results

The results were presented in total displacements and FOS for each scenario.

4.2.1 The Generalized Hoek and Brown failure criterion

The GHB (Hoek et al., 2002) is a failure criterion used in rock masses with poor mechanical properties, it was first developed as a first input parameter for the design of deep excavation and tunnels. The main features of the GHB criterion is the assignation of mechanical properties to rock masses basis on a reduction of the mechanical properties of intact rock. Mechanical and physical characterization of intact rock was developed in tprevious section, the reduction of its properties is based on the particular characteristics of the rock mass (e.g. height, type of rock, surface) and discontinuities (e.g. separation, filling).

The parameters considered by GHB criterion could be summarize in six as follow:

1) Strength of intact rock
2) Bulk density of intact rock
3) Quality of the rock mass by field observation with the use of GSI
4) Type of rock that conform the rock mass
5) Surface quality of the rock mass; for natural slopes could be related with weathering, while in anthropogenic is related with the method of excavation (e,g, TNT, mechanical methods)
6) Geometrical characteristics of rock mass face (e.g. orientation, height)

The GHB criterion aim is to determine the principal stresses (σ_1; σ_3) that acct in the complete rock mass. That behavior of rock mass is represented by the next equation.

$$\sigma_1' = \sigma_3' + \sigma_{ci}\left(m_b\frac{\sigma_3'}{\sigma_{ci}} + s\right)^a \quad (8)$$

Where:

σ'_1 and σ'_3 are the principal stresses of the rock mass

σ_{ci} is the UCS of intact rock

m_b is the reduced value of the material constant m_i that depends on GSI and disturbance factor D (see appendix)

s and a are the constants of rock mass (see appendix)

Also, the GHB criterion make a relation between the MC parameters (cohesion and friction angle) since the most software simulators are based on this last. These parameters are given by the next equations:

$$\emptyset' = sin^{-1}\left[\frac{6am_b(s+m_b\sigma_{3n}')^{a-1}}{2(1+a)(2+a)+6am_b(s+m_b\sigma_{3n}')^{a-1}}\right] \quad (9)$$

$$c' = \frac{\sigma_{ci}[(1+2a)s+(1-a)m_b\sigma_{3n}'](s+m_b\sigma_{3n}')^{a-1}}{(1+a)(2+a)\sqrt{\left[1+\frac{6am_b(s+m_b\sigma_{3n}')^{a-1}}{(1+a)(2+a)}\right]}} \quad (10)$$

Where:

Ø′is friction angle of the rock mass

c′ is the cohesion of the rock mass

σ'_{3n} is the normal stress of rock mass (see Appendix)

Finally, another important paramerer given by the GHB criterion and which is essential in the numerical modeling of rock masses, is the deformation modulus of the rock mass (*Em*). The equation that represent this is given follow:

$$E_m[GPa] = \left(1 - \frac{D}{2}\right)\sqrt{\frac{\sigma_{ci}}{100}}\,10^{GSI-10/40} \qquad (11)$$

4.2.2 Seismic acceleration values

Slope failure may occur due the inertia generated by a seismic event. This inertia could be well represented by a force expressed in a seismic coefficient (*k*). This type of analysis is called: pseudo-static analysis. This analysis assume that seismic forces are proportional to the sliding-mass and are expressed in terms of gravity-times. (Suarez, 1978).

This investigation use micro-tremors as the source for the evaluation of the dynamic characteristic of subsoil. This technique permit us to know the natural period of movement without no necessity of a seismic event. Two points the zone were used for the validation of the dynamic response of the study zone (Fig. 21 and Fig. 20), inversion of Rayleigh wave ellipticity curves were use in order to know the velocity structure of the subsoil (Vazquez-Rosas., 2011). Then, the response spectrum as well as the PGA of the site were estimated with the use of PRODISIS (www2.ineel.mx/prodisis/es/prodisis.php). This software estimates the S-wave propagation speed (v_s) in an equivalent stratum (H_s). The resulting value for were v_s=1277.72 m/s and H_s=421.6 m. According with Fig. 21 the ground type correspond to: Type I, which represent a rocky ground with no dynamic amplifications. The

knowledge of the type of ground was used to determine the F_{sit} (Table 2). Then the maximum seismic acceleration of the ground was obtained with (12)

$$a_0 = 1.5 a_0^r F_{sit} \qquad (12)$$

Where:

a_0*: seismic acceleration (cm/s*^{2}*)*

a_0^r*: maximum acceleration of the rocky ground (cm/s*^{s}*)(* a_0^r*=95.73 cm/s*^{s} *for the zone)*

F_{sit}*: site factor which depends of the seismic zone (zone B) and ground type (Table 2)*

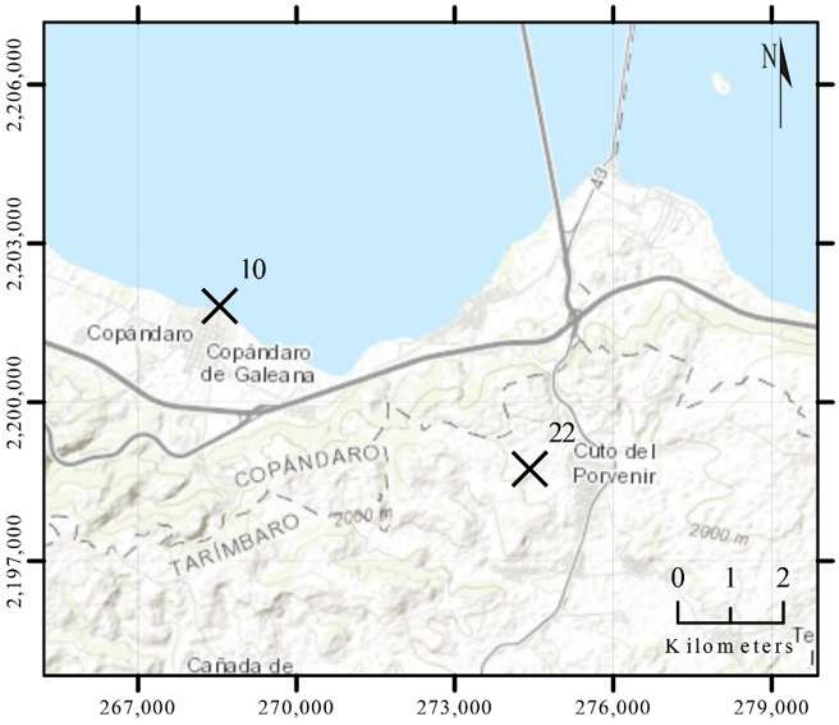

Fig. 21 Location of the seismic inversions

Finally, the seismic coefficient was calculated with (13)

$$k_{x,y} = a_0/g \qquad (13)$$

Where:

$k_{x,y}$: seismic coefficient in x,y direction.

g: gravity acceleration (cm/s^2)

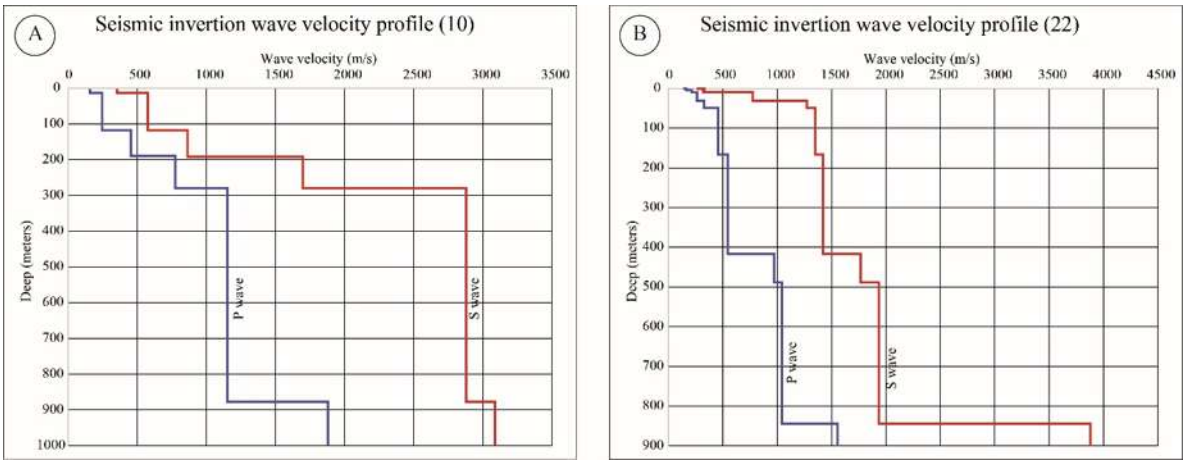

Fig. 22 Wave velocity profile obtained by the method of seismic inversion (Vazquez-Rosas, unpublished data)

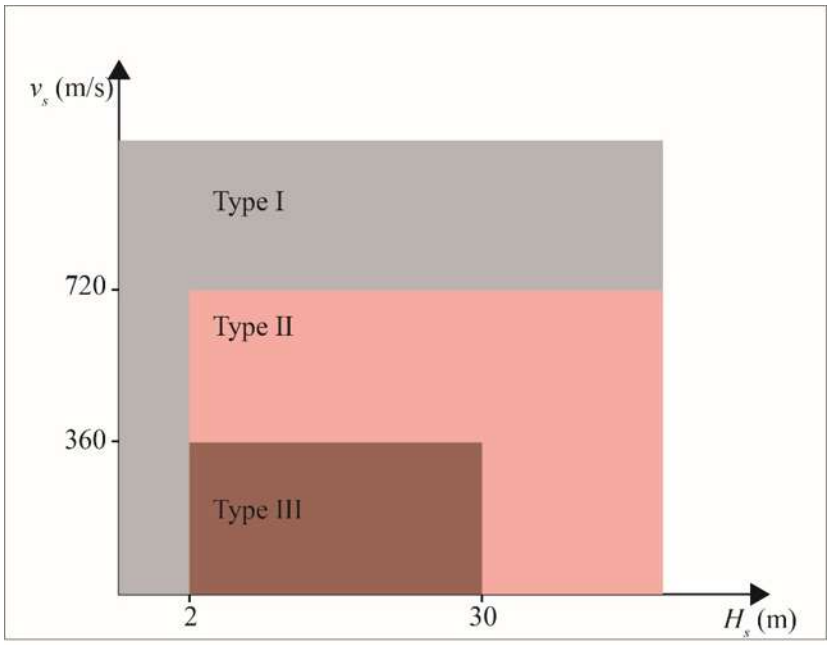

Fig. 23 Seismic microzonification chart. Taken from (Colunga and Mena, 2015)

Table 3 Determination of the F_{sit} according with type of ground and seismic zone (*Colunga and Mena 2015)*

	Type I	Type II	Type III
Zone A	F_{sit}=1.0	F_{sit}=2.6	F_{sit}=3.0
Zone B	F_{sit}=1.0	F_{sit}=2.6-0.2((a_0^r-50)/50)	F_{sit}=3.0-0.3((a_0^r-50)/50)
Zone C	F_{sit}=1.0	F_{sit}=2.4-0.3((a_0^r-100)/100)	F_{sit}=2.7-0.4((a_0^r-100)/100)
Zone D	F_{sit}=1.0	F_{sit}=2.1-0.5((a_0^r-200)/290)	F_{sit}=2.3-0.6((a_0^r-200)/290)

4.2.3 Precipitation values

Precipitation have been considered a trigger factor for slope failures. The saturation of materials affect directly not only their mechanical behavior, but also, the increase of the mass and pore pressures generations. The Cuitzeo-Region have registered precipitation of more than 50 mm on rainy seasons (www.smn.cna.gob.mx). Historical data from meteorological station were collected in order to consider the maximum rain in our numerical model. Data of the maximum registered precipitation was obtained from the "Mexican Meteorological Survey" (SMN).

Table 4 Santa Rita historic precipitation (extreme values)

Santa Rita Station (extreme precipitation values)

Lat: 19.9039° Long: -101.2611°

	Start year	End year	Total years	Max precipitation (mm)	Date
Ene	1965	2016	51	75	09/01/1967
Feb	1965	2016	51	30	18/02/1981
Mar	1967	2016	49	40	14/03/2015
Abr	1966	2016	50	23	05/04/1973
May	1966	2016	50	40	24/05/1982
Jun	1965	2016	51	52	20/06/2007
Jul	1967	2016	49	85	29/07/1976
Ago	1966	2016	50	80	13/08/1969
Sep	1966	2016	50	90	18/09/1969
Oct	1964	2015	51	36	09/10/2004
Nov	1964	2015	51	35	02/11/1972
Dic	1964	2015	51	23	04/12/2015

The maximum values of precipitation were used in conjunct with the phreatic level of the zone. Phreatic level was proposed in accordance with the Cuitzeo Lake water table.

5. Results

This section presents the most significant results in the investigation. First, the stratigraphy of the slope is described in accordance with the fieldwork. Then, the geomechanical characterization of the different units is presented, the geomechanical characterization was accomplished in accordance with the fieldwork-data, laboratory tests and the use of the GHB criterion. Finally, the results from the different scenarios in the numerical modeling are presented, both the LEM and the FEM with GeoSlope and Plaxis 2D respectably.

5.1. Statigraphy

The stratigraphy of the zone is conformed by the intercalation of pyroclastic products and andesitic lavas. The geology of the study zone were divided in 4 stratigraphic columns (Fig. 1). The main ignimbrite sequence correspond totally to the stratigraphy of the slope. Stratigraphic correlation were done with the description of hand samples as follow:

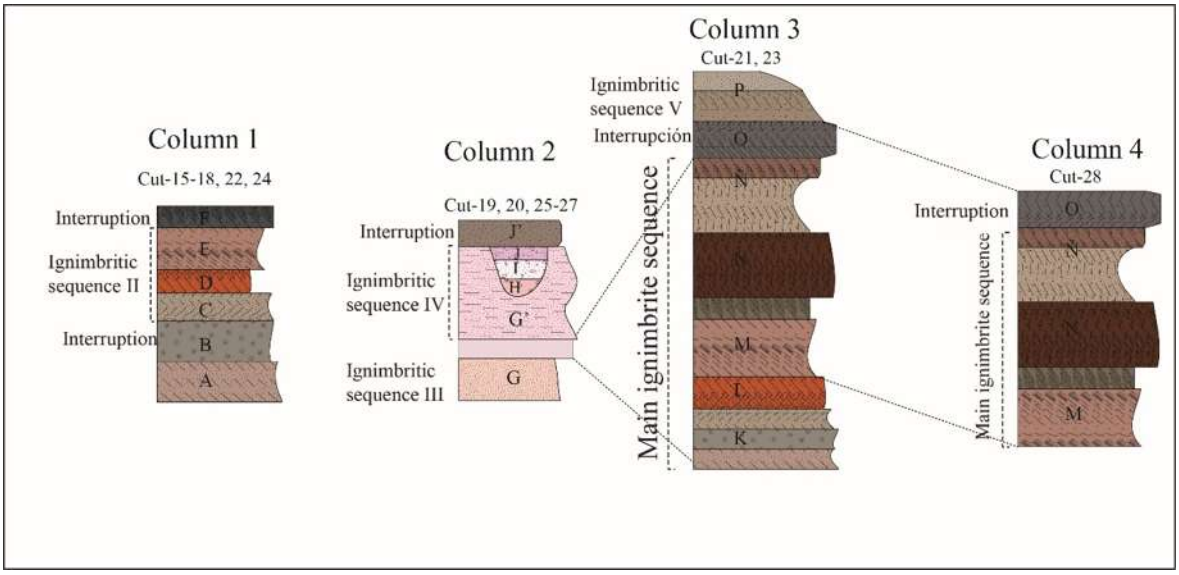

Fig. 24 Stratigraphic columns accomplished in the study zone. The main ignimbrite sequence

Column 1

Unit A: Pink ignimbrite which alteration turns to a white color, massive texture and poor-medium welded degree. It is conformed by yellow pumice size coarse lapilli, gray and red lithics in a fine ash matrix.

Unit B: Gray lava flow which is much fractured in a rock mass level. It has a porphyritic texture whit phenocrysts of plagioclase, quartz and amphibole. It has also some rounded embed whit phaneritic texture and phenocrysts such as plagioclase, amphibole and quartz (Fig. 24A).

Unit C: Pyroclastic flow deposit, pink color which alteration turns to white, massive and high welded degree. It is formed by white fiamme four centimeters long, sharp red-gray lithics size coarse lapilli. This unit also present high presence of crystals such as plagioclase, quartz and amphibole in a welded matrix (Fig. 24D).

Unit D: Pyroclastic flow deposit, pink-white color. Massive and medium welded degree. White fiamme were observed and sharp lithic fragments that variate from red to gray. It contain crystals of plagioclase, quartz and amphibole.

Unit E: Pyroclastic flow deposit very similar to unit A (Fig. 24B)

Unit F: Lava flow deposit, gray color and highly fractured. It presents spheroidal alteration and fractures filled with calcite. It has porphyritic texture with phenocrysts of quartz, amphibole and plagioclase (Fig. 24C).

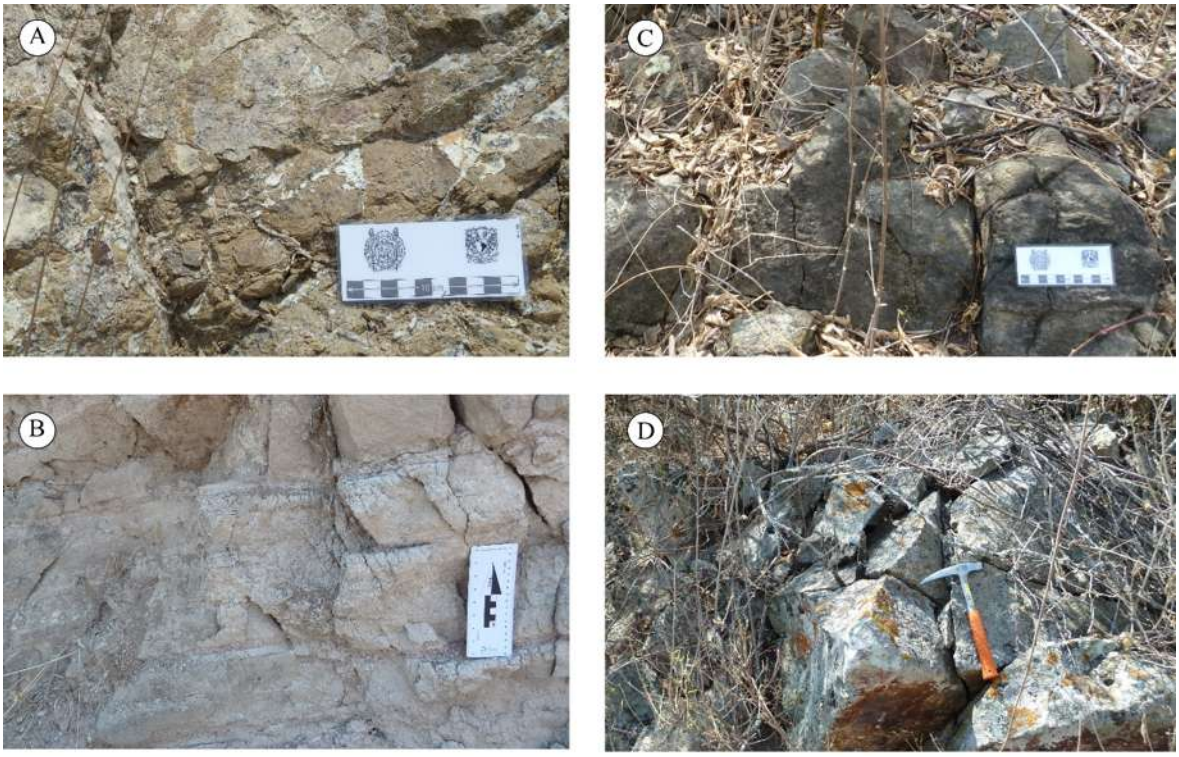

Fig. 25 Rock units of columns 1. A) andesitic gray lava affected by hydrothermal alteration (Unit B); B) Pyroclasic flow medium-welded degree; C) Lava flow deposit from Unit F; D) Massive ignimbrite high-welded degree

Column 2

Unit G: Ignimbrite deposit, pink to purple color, massive and medium welded degree. Poor content of lithics, these are black-brown color. Some phenocrysts such as amphibole.

Unit G': Stratified deposit pink color. It is constituted by the intercalation of pyroclastic flows medium welded degree. In general, deposits consist in yellow pumice that variates in size from fine to medium lapilli, it has sharp lithics red-gray and some green size block, all of these within a medium ash matrix.

Unit H: Stratified remobilized deposit, pink-yellow color, poor welded degree. It is composed by rounded rock blocks of maximum thirty centimeters within a coarse ash matrix.

Unit I: Remobilized deposit white color whit some gray-red tones, massive and highly wended. It has a considerable amount of phenocrysts of quartz, feldspars, amphibole and biotite? All of these is embedded in a medium ash matrix.

Unit J: Stratified deposit pink-yellow color, massive and a poor medium welded degree. It was no possible reach the layer, since there was not a hand specimen description.

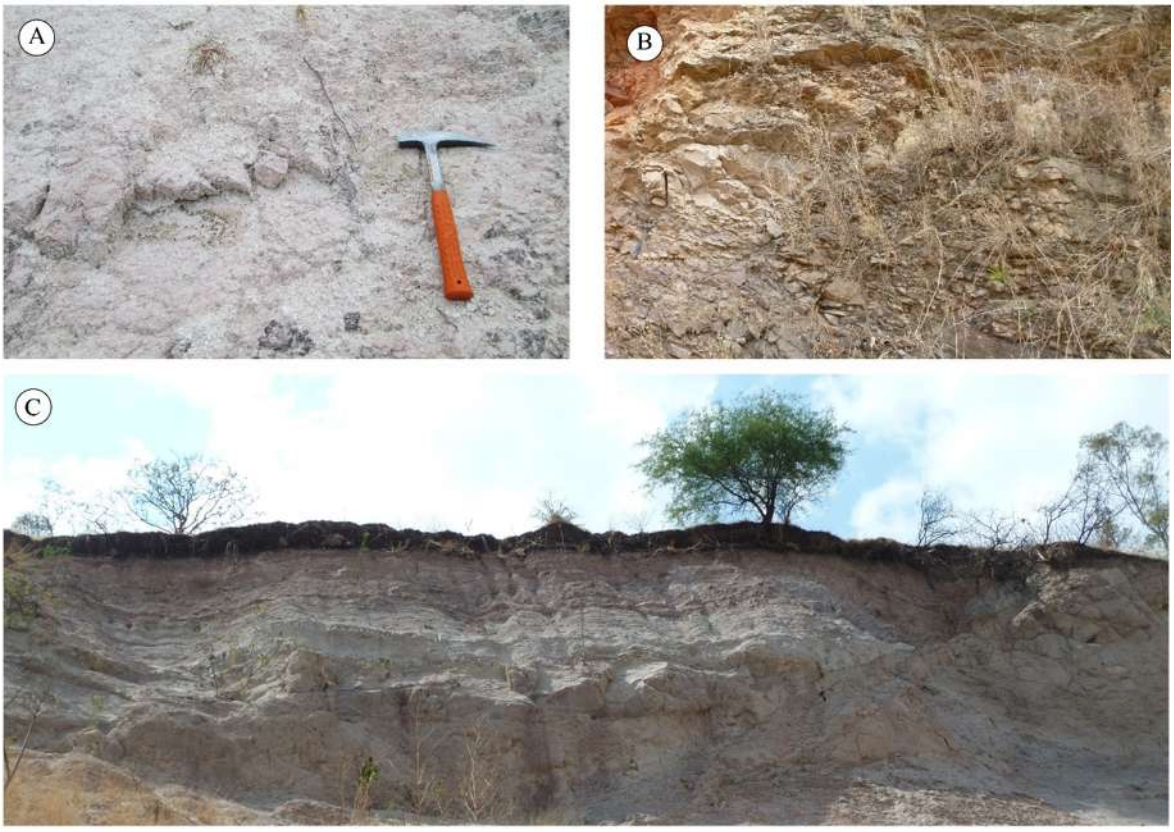

Fig. 26 Rock units of columns 2. A) Unit G from the column which present a poor-welded degree; B)Unit G from the column which present a medium welded degree; C) Stratified isolated flow which is composed by Unit H, I and J

Column 3

This column represent the stratigraphy of the analyzed slope. It include the main ignimbritic sequence which was divided in seven layers. The variation are specially viewed in the welded degree (Fig. 26A) and the apparition of the andesitic lava (Fig. 26B). The complete sequence outcrops in the highway, specifically in Cut-05, Cut 21 and Cut-23 (Fig. 26C). These are described as follows from bottom to the top:

Fig. 27 Outcrops in the highways. A) Unit K which presents a poor welded degree; B) contact between lava and welded ignimbrite; C) General view of Cut-21

K: Stratified deposit, pink color, it is constituted by intercalation of pyroclastic flows, surges and falls. In general, the pyroclastic flows variate from poor to medium welded degree and they present pumice fragments that variate in size from fine lapilli to block. They present plagioclase, quartz, feldspars and amphibole within a medium ash matrix. It was also observed sharp red-gray-green lithics. On the other hand, surges were brittle and a parallel stratification was observed. In some layers were observed acretional lapilli and white pumice in the inner. A few crystals were observed in the surges, some as plagioclase, quartz and amphibole. The las layer corresponds to a fall deposit without visible gradation, dark color and approximately two centimeters thickness (Fig. 27A).

L: Pyroclastic flow deposit, red color, massive, highly welded but also highly fractured. It was formed by black fiamme up to five centimeters long and sharp gray-red lithics. Phenocrysts of plagioclase, quartz and amphibole (Fig. 27C).

M: Stratified ignimbrite deposit, pink color which is constitute by the intercalation of pyroclastic flows and surges. Pyroclastic flows are high weathered, massive and brittle. Sharp

dark-red lithic were observed, as well as phenocrysts of plagioclase, feldspars and some rusty red crystals, the above within a medium-fine ash matrix. On the other hand, surges are characterized by parallel stratification. Layers variated from poor to medium welded and thickness of one to thirty centimeters (Fig. 27D).

N: Stratified deposit, pink-white color, and poor welded degree. It is constituted by the intercalation of pyroclastic flows and surges. Pyroclastic flows are massive and constituted by sharp white pumice and sharp red lithics size fine lapilli. Also were observed rounded red-gray-yellow lithics size block. Otherwise, surges present parallel stratification with layers up to twenty-five centimeters.

O: Lava flow deposit, dark-gray color it turns red in some weathered parts of the outcrop and it is highly fractured. Also, filled vesicles were observed, the fill material is color yellow-green. It presents aphanitic texture with less rusty micro-phenocrysts within a micro crystalline matrix of plagioclase and pyroxenes (Fig. 27B).

P: Stratified ignimbrite deposit, pink-white color. It is constituted by the intercalation of pyroclastic flows and surges. Pyroclastic flows are massive, poor-medium welded and highly fractured with some spheroidal alteration. It is composed by sharp white-yellow pumice, size medium-coarse ash, also sharp red-gray lithics size fine lapilli. It were observed minerals such as quartz, plagioclase and amphibole in a fine ash matrix. Moreover, surges present parallel stratification and the layer thickness is up to 1ten centimeters. Pumice fragments were observed, size medium ash and less sharp red-gray lithics.

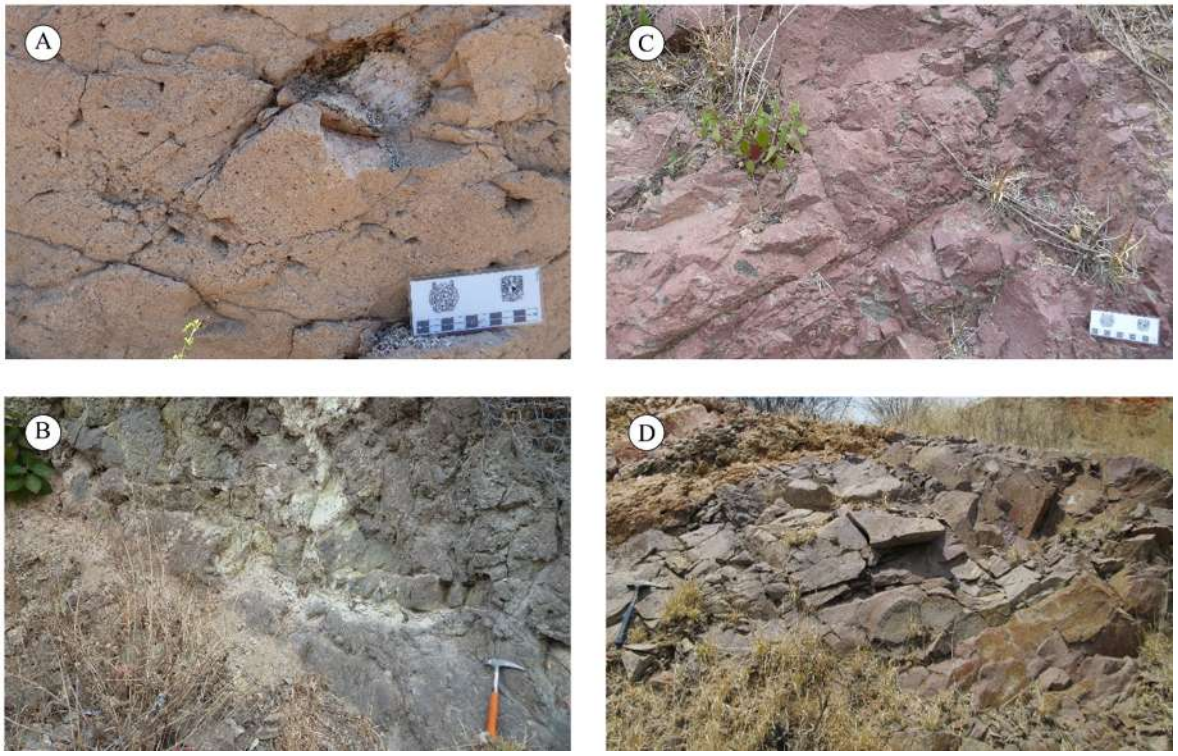

Fig. 28 Rock units of Column 3. A) Unit K were acretional lapilli were observed; B) Lava deposit which is highly fractured; C) Unit L which is an ignimbrite highly fractured and welded; D) Unit M which present a medium welded degree.

Column 4

M: Pyroclastic flow deposit, pink-white color, massive and poor-medium welded degree. It contents sharp white pumice, size medium lapilli as well as red-dark gray lithics. Crystal components observed correspond to plagioclase, quartz and rusty Fe-Mg materials, all the above embedded in a medium welded ash matrix.

N: Pyroclastic flow, red color, massive and high welded degree Fig. 28A,C. It has white-gray fiamme (Fig. 28B) up to three centimeters long, less yellow-gray lithics and crystals such as plagioclase, feldspars-K, quartz and amphibole, all the above within a welded matrix.

Ñ: Stratified deposit with alternation between pyroclastic flows and surges. Pyroclastic flows are gray-white and poor medium welded degree. They content white pumice and black-red-oranges lithics. Plagioclase, quartz and some rusty Fe-Ti were

observed in a fine medium matrix. On the other hand, surges has parallel stratification and thickness up to thirty centimeters. White pumice fragments were observed as well as some black-yellow lithics.

O: Lava flow deposit, dark-gray color with phenocrysts of altered quartz (Fig. 28D).

Fig. 29 Rock units of Column 4. A, C); outcrop were unit N were observed with high welded degree; B) gray fiamme from unit N; D) Lava deposit.

5.2. Geomechanical characterization of rock masses

In this section are included the results from the geomechanical classification in the different rock units that composed the main ignimbrite sequence.

The observation in fieldwork included the estimation of the GSI. In general all the units analized present values less than 50 (Fig. 29). This situation is due two main factors. 1) Rigid rocks (welded ignimbrites and lava) present a lot fractures (Fig. 29A,B) and 2) Medium-poor welded ignimbrites does not present a lot of fractures, however, they are brittle or more suceptible to weathering (Fig. 29C,D).

Fig. 30 GSI values observed in fieldwork. A) Welded ignimbrite with high welded degree and very fractured; B) contact between blocky lava and brittle ignimbrite; C) medium welded degree ignimbrite and highly blocky; D) Brittle ignimbrite with low GSI

Physical characterization of intact rock include the accomplished of three tests: bulk density test, real density test and permeability tests. ρ_{bulk} of ignimbrites variates from 1200 Kg/cm^3 to 1900 Kg/cm^3. On the other hand, andesite sample results in a $\rho_{bulk=}$ 2650 Kg/cm^3. Real density ranges from 2036 Kg/cm^3 to up to 3000 Kg/cm^3 for ignimbrites and for andesite a ρ_{real}=2730 Kg/cm^3. The knowledge of these two physical properties was used in the

determination of the porosity. All these data are summarized in Table 4, also are included the results from the PLSI.

Table 5 Summarize of the physical and mechanical properties. Is_{50}: point load index η: porosity. *(Pola et al., 2016)

Unit	Id	I_{s50}	*UCS*	$\rho_{part}(Kg/m^3)$	$\rho_{bulk}(Kg/m^3)$	η	*GSI*	*GHB parameters*	
								D	m_i
Andesite	Cut-04	1.344	35.870	-	2650.000	-	30-40	0.8	25
Ignimbrite	Cut-07	-	11.330	2372.000	1512.000	36.26%	30-40	0.8	13
Ignimbrite	Cut-12	1.130	23.729	2470.000	1283.000	48.06%	45-55	0.8	13
Ignimbrite	Cut-13	0.458	6.487	3361.000	1590.000	52.69%	35-45	0.8	13
Ignimbrite	Cut-14	0.699	10.565	2303.000	1910.000	17.06%	40-50	0.8	13
Ignimbrite	mpa*	-	4.330	2337.097	1449.000	38.00%	30-40	0.8	13
Ignimbrite	mpl*	-	8.290	2415.152	1594.000	34.00%	30-40	0.8	13
Ignimbrite	spl-a*	-	9.570	2036.232	1405.000	31.00%	30-40	0.8	13
Ignimnbrite	spl-b*	-	8.930	2092.754	1444.000	31.00%	30-40	0.8	13

Permeability of intact rock was obtained in a permeameter type column. Permeability is long dependence of porosity. Only one permeability test could be carried out and the permeability to all rocks was given in the same way. The results for permeability throw a mean value of K_L=0.4 mDa (). This test depend in long way of the flow during the test. This results were converted to obtain the velocity of the flow throw the rock. Results are showed in Table 5 for each rock unit.

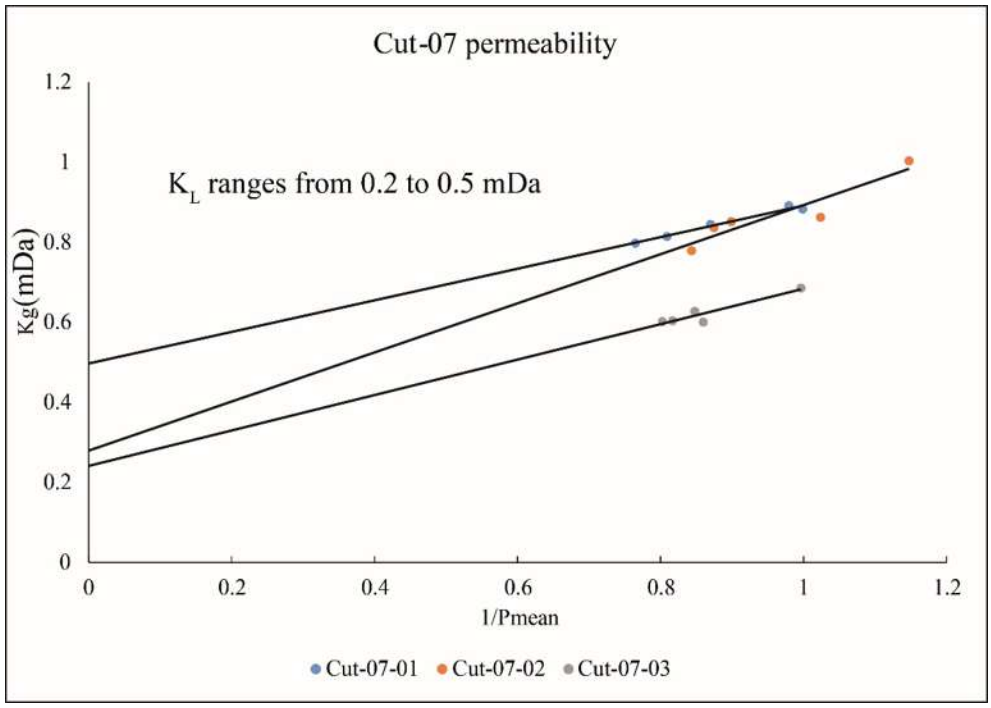

Fig. 31 Permeability test on an ignimbritic sample. Three test on the same unit were carried out.

Table 6 Hydric results. υ=dynamic water viscosity; e=void ratio; ρ_{sat}=saturated density; K_L=permeability; $K_{x,y}$=flow throw the rock

Hydric results						
Unit	Id	υ (Kg/m s)	e	ρ_{sat} (Kg/m^3)	K_L (m^2)	$K_{x,y}$ (m/day)
Andesita	Cut-04		0.03	2679.30	4.00E-16	0.42
Ignimbrita	Cut-07		0.57	1874.56	4.00E-16	0.42
Ignimnbrita	Cut-12		0.93	1763.57	4.00E-16	0.42
Ignimnbrita	Cut-13		1.11	2116.93	4.00E-16	0.42
Ignimnbrita	Cut-14	0.0008910	0.21	2080.65	4.00E-16	0.42
Ignimnbrita	mpa*		0.61	1829.00	4.00E-16	0.42
Ignimnbrita	mpl*		0.52	1934.00	4.00E-16	0.42
Ignimnbrita	spl-a*		0.45	1715.00	4.00E-16	0.42
Ignimnbrita	spl-b*		0.45	1754.00	4.00E-16	0.42

The determination of the mechanical parameters of the complete rock masses were carried out by the use of the GHB criterion The combination of the observation on fieldwork and laboratory test on intact rock results in the mechanical properties of the rock mass. The results are summarized in Table 6.

Table 7 Mechanical properties of rock masses. *(Pola et al., 2016)

Unit	Id	Rock mass mechanical properties		
		c_m (MPa)	φ_m (°)	E_m (MPa)
Andesite	Cut-04	0.61	27.86	1515.36
Ignimnbrita	Cut-07	0.21	19.19	851.66
Ignimnbrita	Cut-12	0.40	32.31	2922.75
Ignimnbrita	Cut-13	0.20	17.67	859.36
Ignimnbrita	Cut-14	0.31	21.51	1462.47
Ignimnbrita	mpa*	0.13	14.25	526.50
Ignimnbrita	mpl*	0.19	17.11	728.50
Ignimnbrita	spl-a*	0.19	18.63	782.72
Ignimnbrita	spl-b*	0.18	18.08	756.10

5.3. Numerical modeling

This section presents the results for the numerical simulations. The results are divided in the four scenarios (static, dynamic, precipitation and dynamic+precipitation) for FEM and LEM. Results from FEM are given in deformed mesh as well as the maximum displacements along the slope and the FOS. Otherwise, LEM results are just given the crital slide surface and the FOS.

5.3.1 Plaxis 2D

The first scenario analyzed was the static. This means that only mass and gravity force were acting. The deformation was only along the slope face, the top of the slope ddid not present settlements, this type of failure may be classified as a general fault. The maximum displacements allong the slope was 2.65 meters. The calculated FOS=1.400 indicates that under static conditions the slope is stable (Fig. 31).

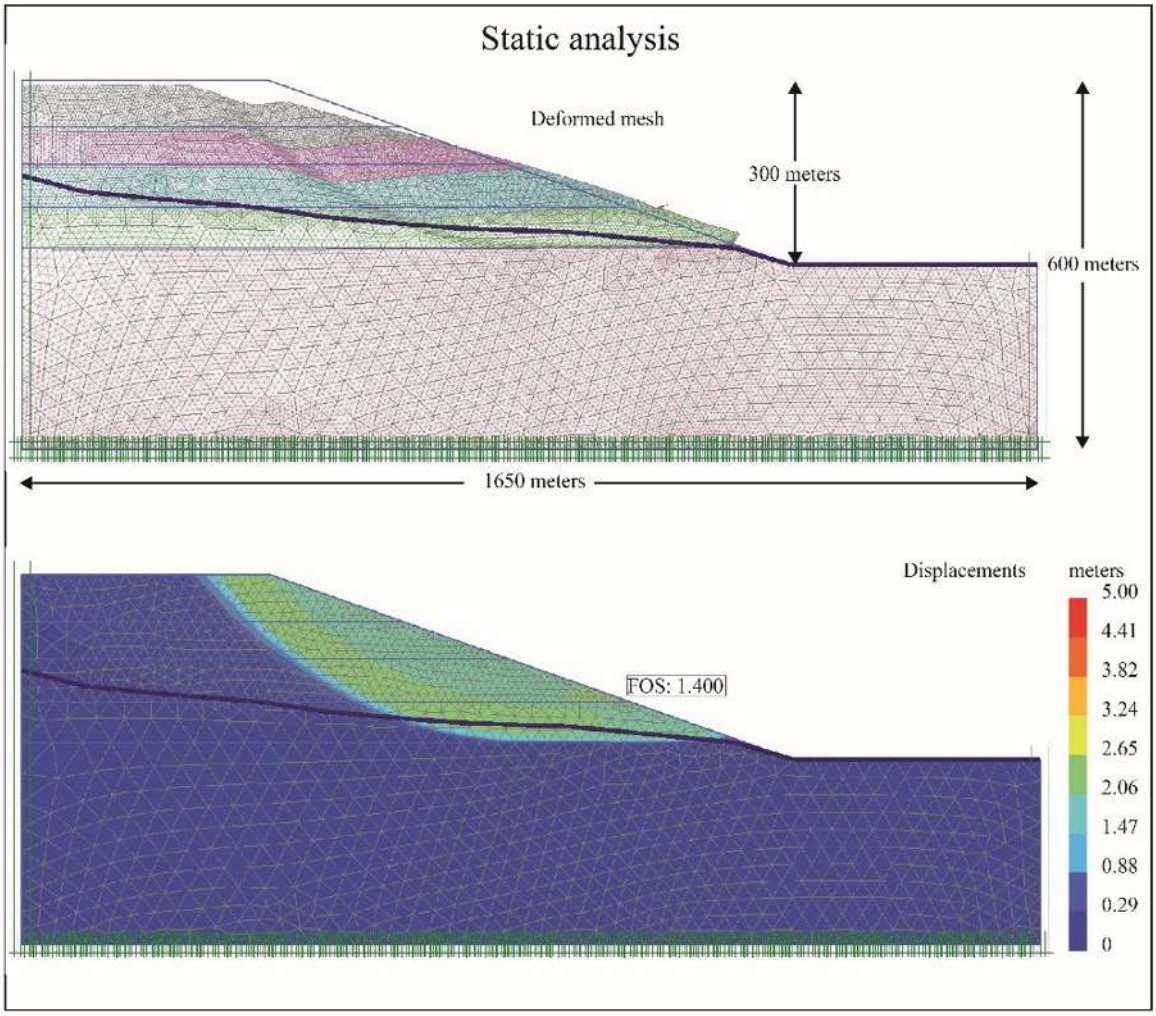

Fig. 32 Static results using Plaxis 2D. Deformed mesh (top) and displacements (bottom).

The second scenario analyzed was the slope under a dynamic load, this is represented by an accelerationin X and Y direction of 0.15 g. In diference with the static analysis, the deformed mesh of this scenario shows 2 tifferent movements. The first displacements occur on the top of the slope in Y direction. This displacement are classic in a seismic event, the materials tend to consolidates due the seismic acceleration. The second displacements occurs due the static conditions, the displacements decrease from the top to the bottom of the slope and the FOS is reduced to 1.014. The value of FOS>1 still indicates stability, however, if we are on a conservative analysis the slope under this dynamic condition indicates a failure (Fig. 32).

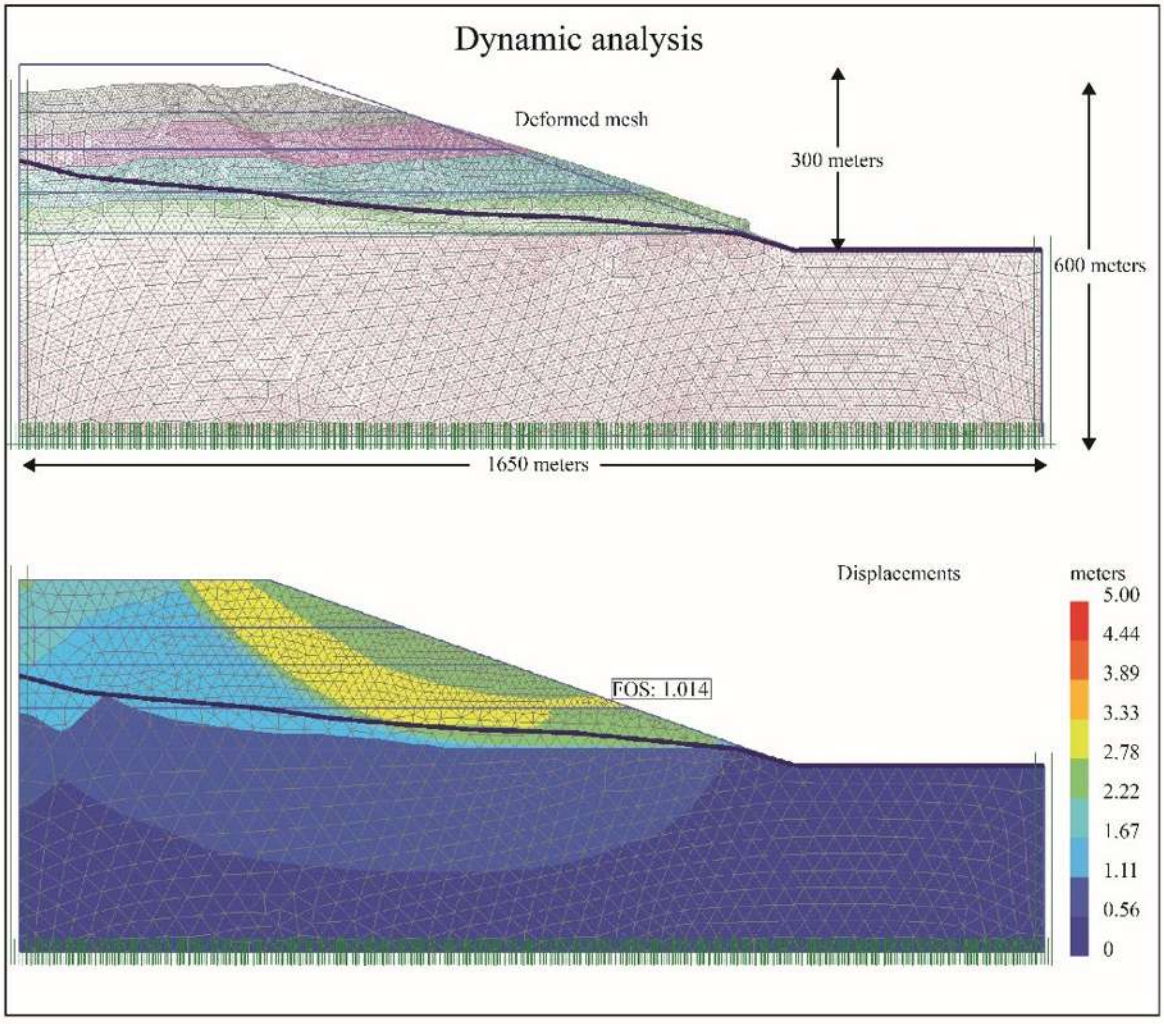

Fig. 33Dynamic analysis in Plaxis 2D

Precipitation analysis is a very particular case. The deformed mesh shows a similar movement that the static analysis, FOS decrease to 1.374 which indicates conditions of stability under conditions of precipitation (0.090 m/day). The displacements are greater than those in the static analysis and even in the dynamic analysis. This may indicates a plastic behavior of the slope, in other words the displacements of the materials does not increase proportionally to the stresses (Fig. 33).

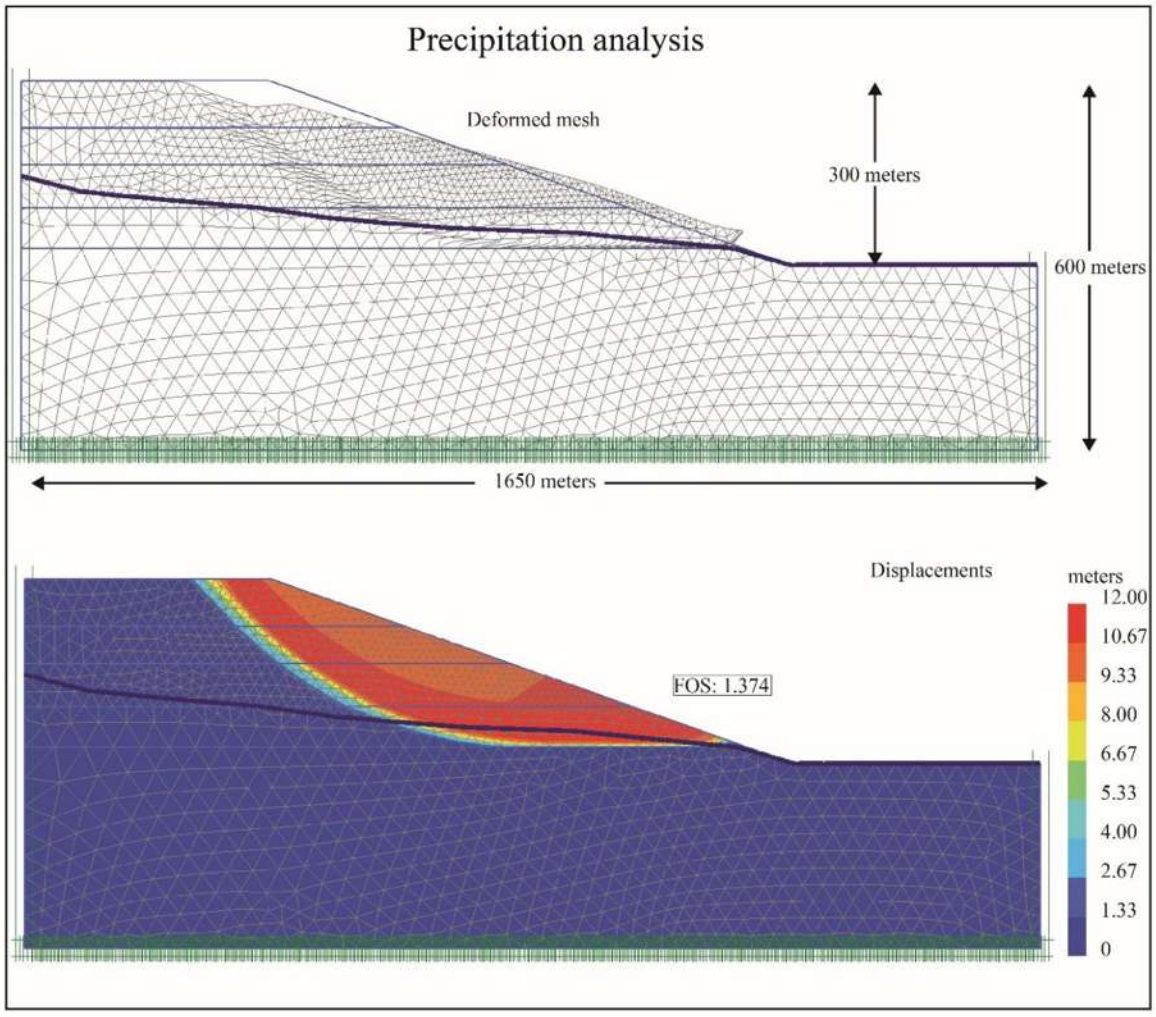

Fig. 34 Precipitation analysis in Plaxis 2D

The consideration of the dynamic force and precipitation was the fourth analysis. Deformed mesh indicates three different movements. First, the settlements due the dynamic force (0.15g) in Y direction, the second movement is due the static conditions, however, this movements present a variation. There was not a unique slide surface, due the precipitation 2 slides surfaces were observed in the deformed mesh, they match deeper forming a unique exist. The FOS was reduced to 1.009 and the maximum displacement of 3.89 meters. This scenario is the most representative of the real conditions observed in fieldwork (Fig. 34).

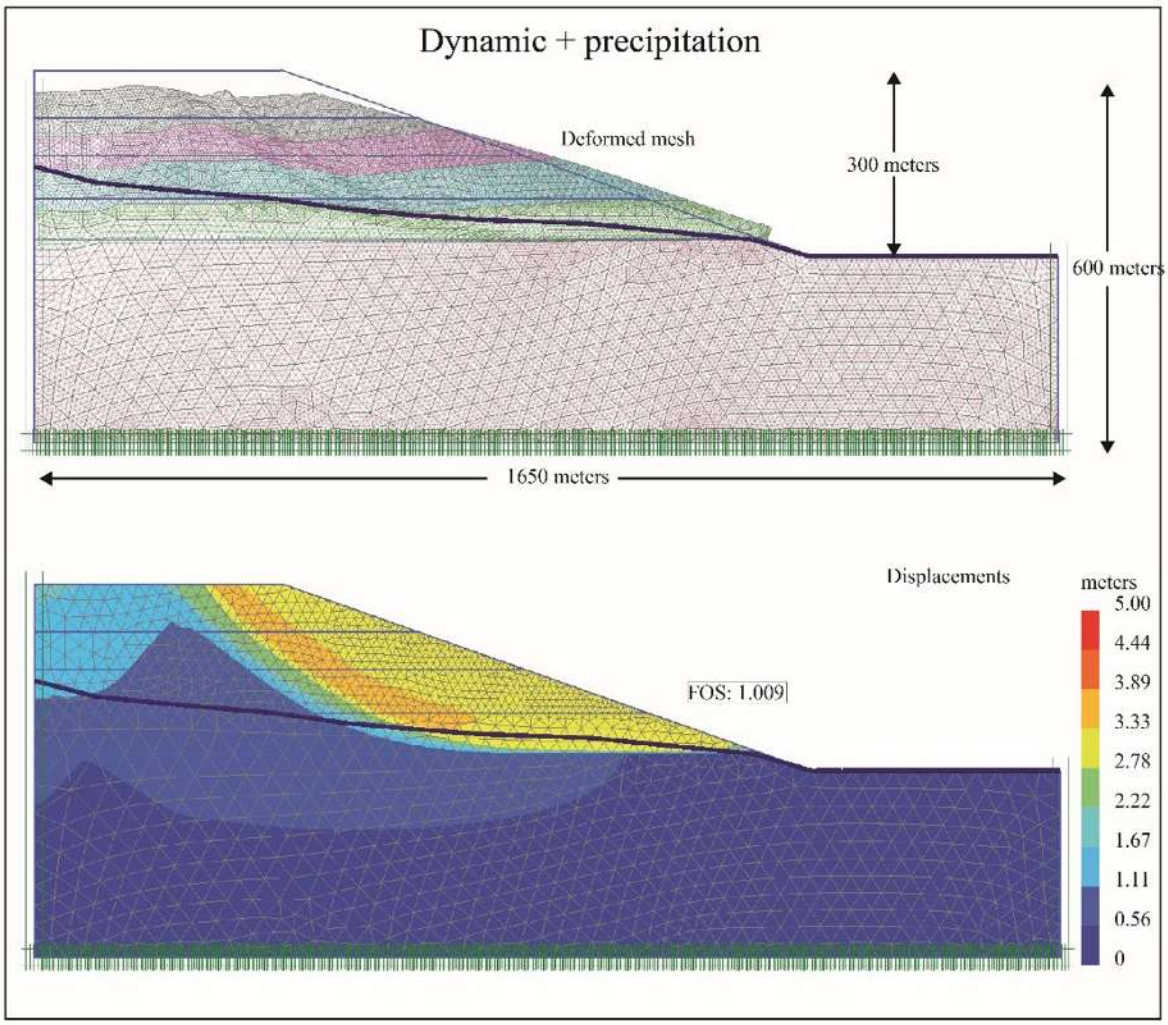

Fig. 35 Dynamic + precipitation analysis in Plaxis 2D

In order to verify the conditions under the FOS decrease under 1.0, the seismic forces were increased to 0.30 and 0.45 in the Y axis. The precipitation conditions were kept similar to the previous analyses, as well as the phreatic level. Deformed mesh confirm the same movements that the previous analysis and they differ in the magnitude of the displacements and the value of FOS. The maximum displacements increase to 3.89 meters and 9.00 meters for the 0.30g and 0.45g respectably. Both cases, FOS was less than 1.0, 0.991 and 0.988 for 0.30 and 0.45 respectably. Whit this data was possible to determine the settlement due seismic acceleration, resulting an approximately value of 35 meters and the depth of the slide surface rounded the 170 meters (Fig. 35 and Fig. 36).

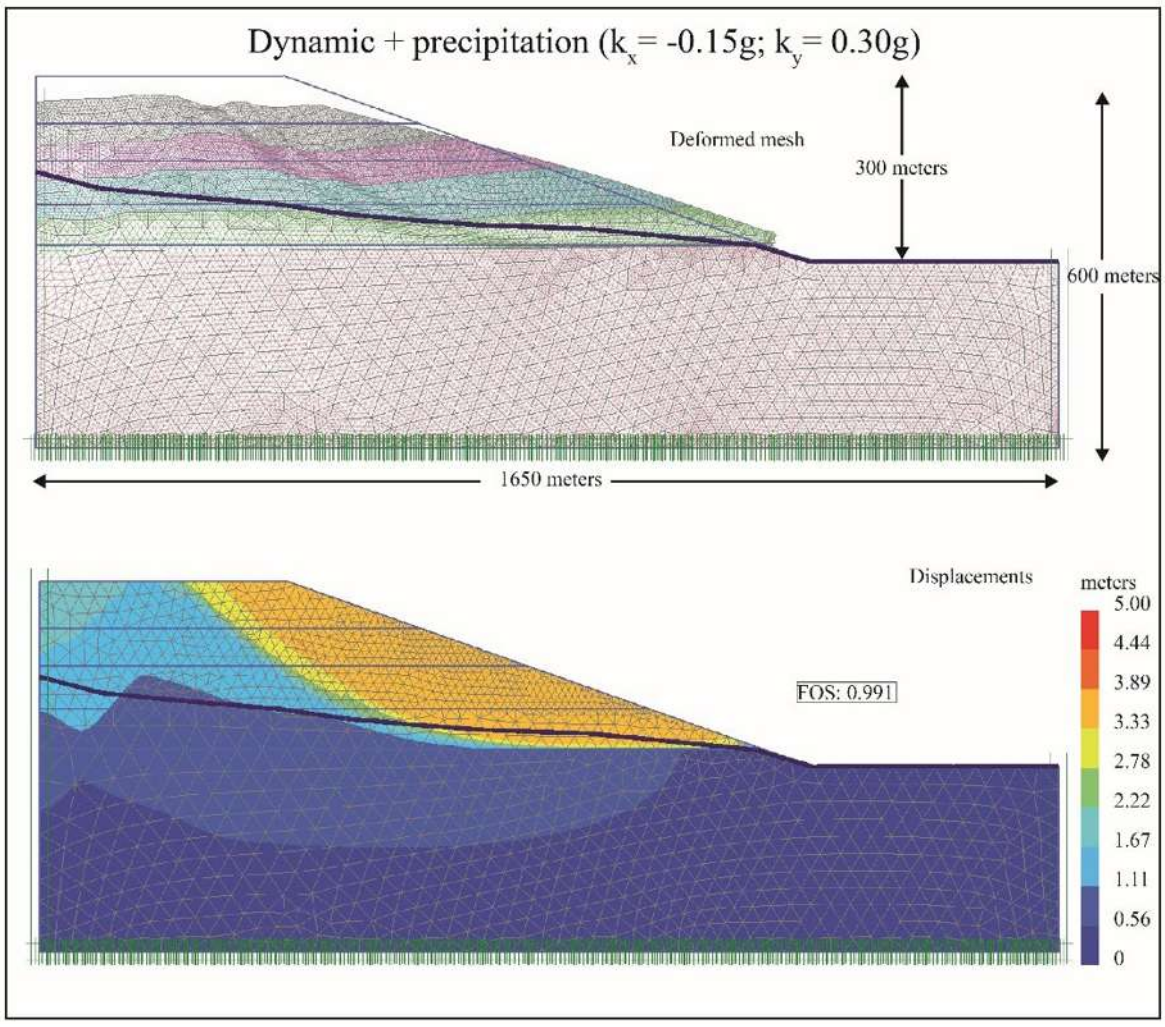

Fig. 36 Model with dynamic acceleration in X=0.15g and Y: 0.30g

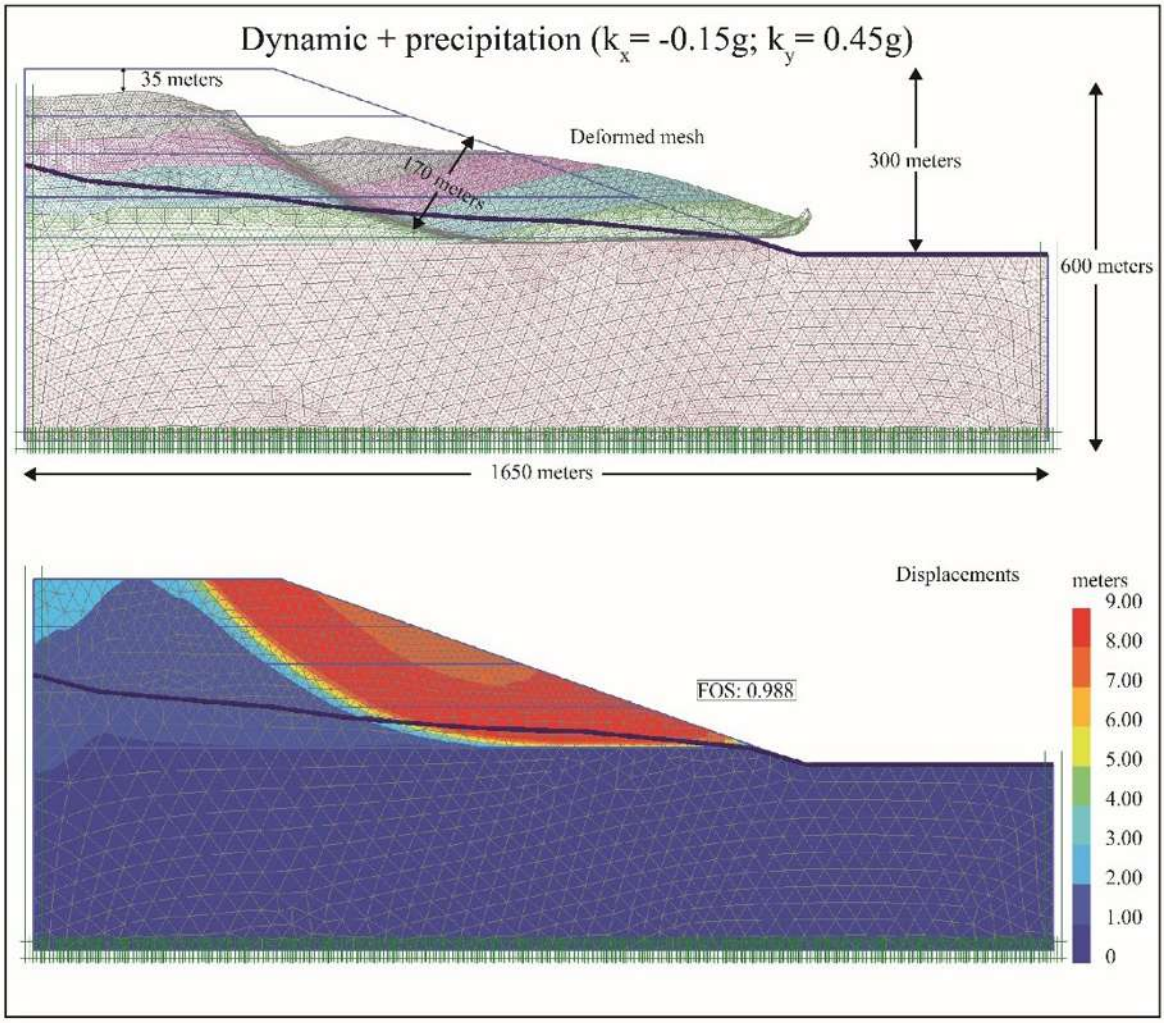

Fig. 37 Model with dynamic acceleration in X=0.15g and Y:0.45g

5.3.2 GeoSlope

The result of the LEM were the expected, FOS was higher in comparison with the anañysis with FEM. The same scenarios were analyzed and the most remarkable difference was in the static scenario. FOS using GeoSlope was 2.24 (Fig. 10) the slide surface match perfectly with the results of Plaxis 2D. Dynamic scenario with GeoSlope results in a FOS= 1.54. The reduction of the FOS in comparison with the static scenario is around 31% (Fig. 11).

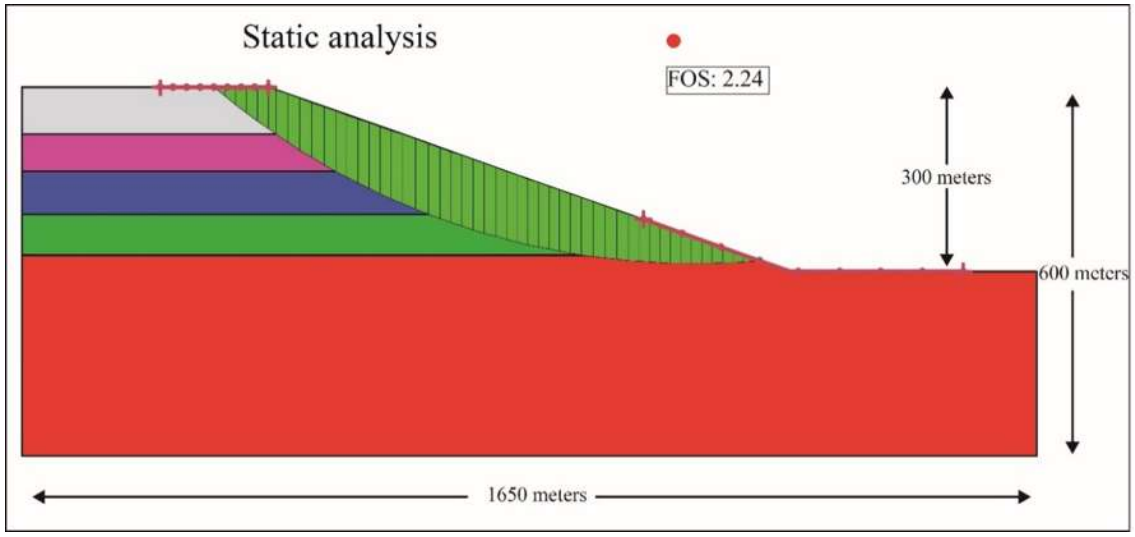

Fig. 38 Static analysis with GeoSlope

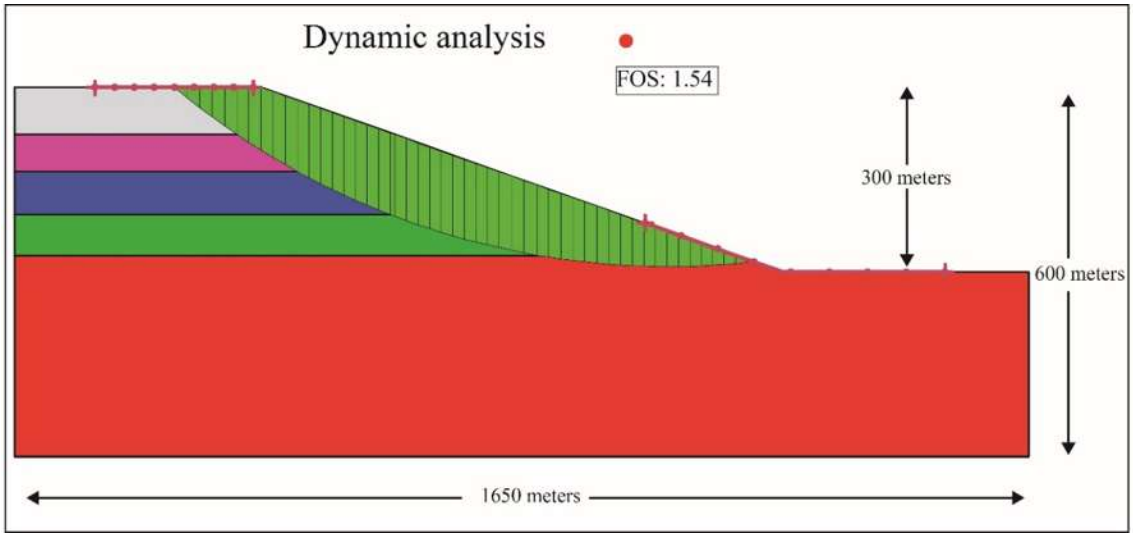

Fig. 39 Dynamic analysis with GeoSlope

It was not possible to include precipitation data on GeoSlope, in that way, the phreatic level was proposed to be acting along the complete slope face (Fig. 12). The results from the combination of precipitation and dynamic load throw a FOS= 1.38. In comparison with the results from FEM, the FOS for GeoSlope was higher, but the critic slide surface correspond in both methods (Fig. 12).

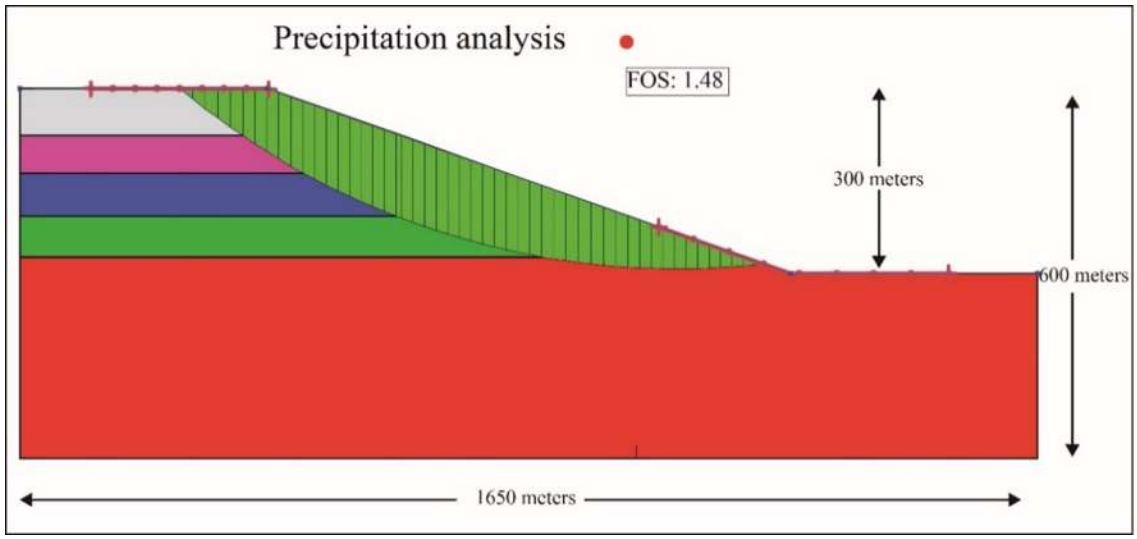

Fig. 40 Precipitation analysis. Phreatic level was proposed along the slope face to simulate a saturated material.

As well as in the FEM, the slope was analyzed with two more seismic acceleration combiataion. First, X=0.15g and Y=0.30g results in a FOS= 1.16. The second combination (X=0.15g; Y=0.45g) results in a FOS= 0.99 (Fig. 14 and Fig. 15).

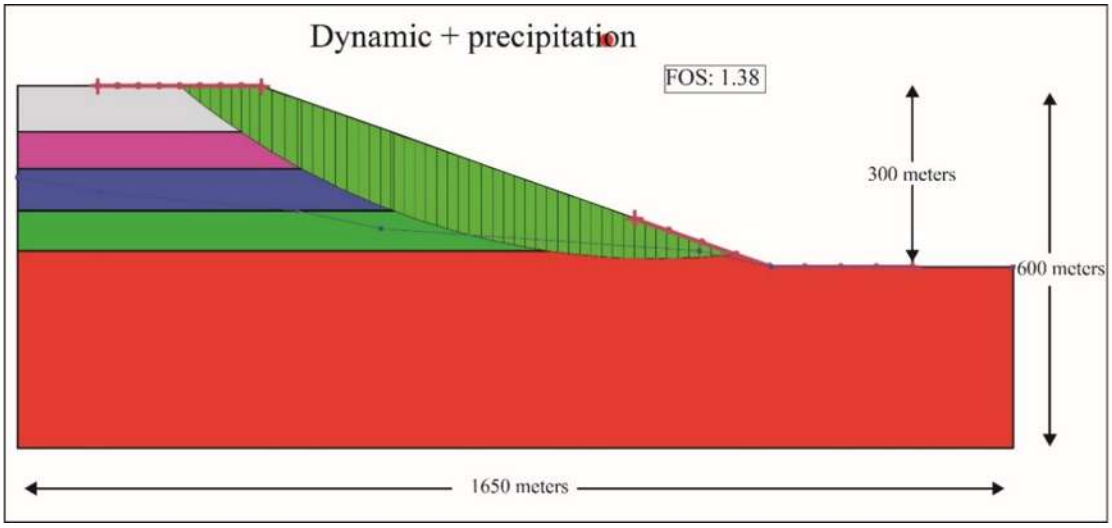

Fig. 41 Dynamic + precipitation analysis with GeoSlope

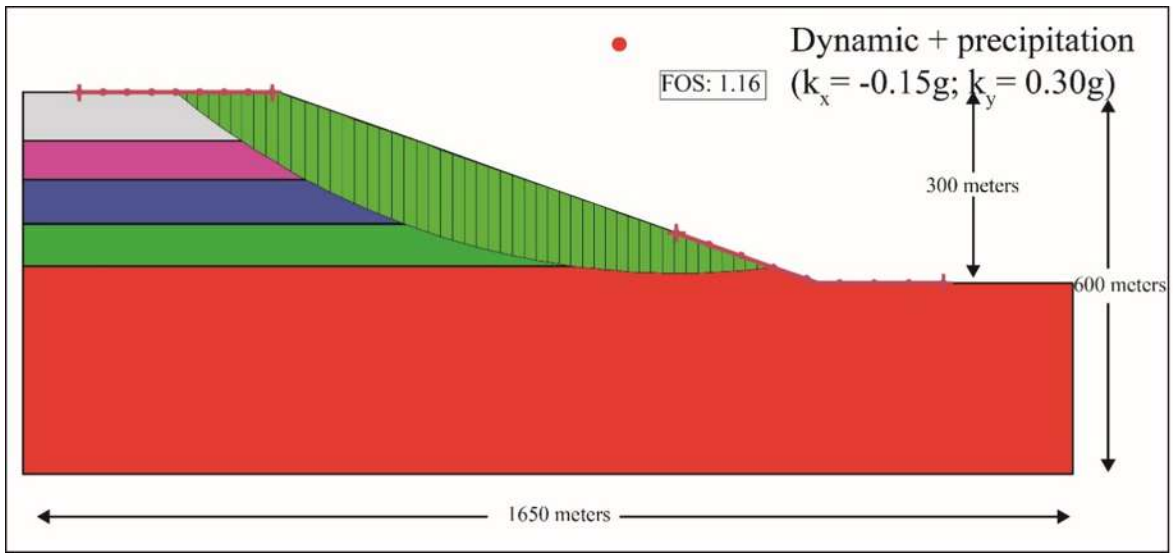

Fig. 42 Dynamic acceleration with kx=0.15g and ky=0.30g

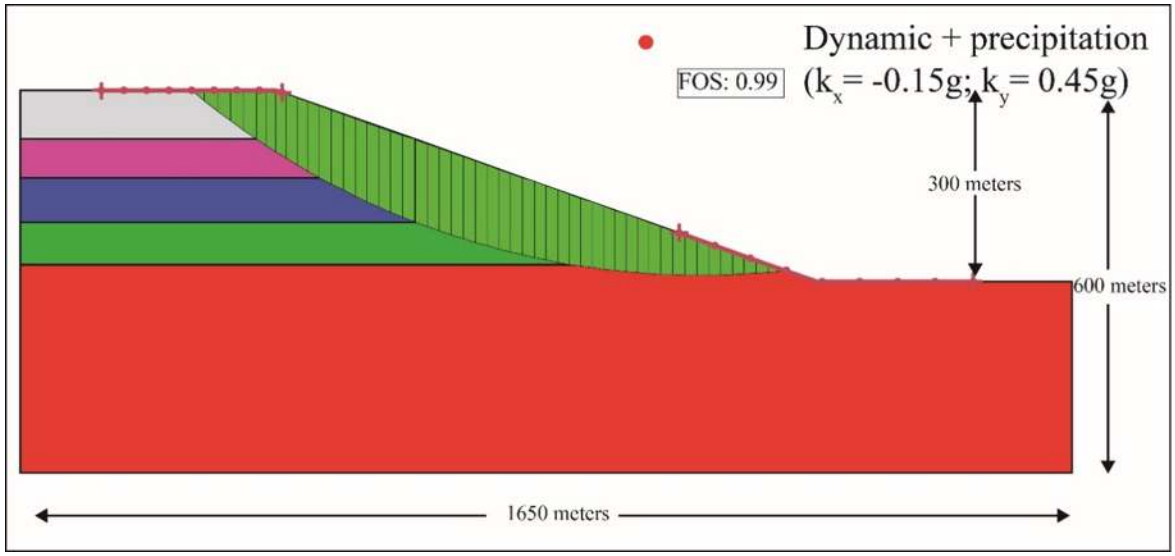

Fig. 43 Dynamic acceleration with kx=0.15g and ky=0.45g

6. **Discussions**

All the slope stability analyses are long influenced by the geology, geomorphology, weather conditions and also by the geomechanical characteristics of the materials.

The assignation of mechanical properties to intact rock is relatively easy comparing with the assignation of mechanical properties to rock masses. Laboratory tests are enough for the characterization of intact rock, however, there is not a direct method for determining the physical and mechanical properties of rock masses. Empirical equation such as the GHB and the MCC have been developed for estimate this parameters but they are long dependence of the human criteria.

The effect of the scale in the analysis of slope stability is very important. As mentioned above, Cuitzeo-Region have been characterized by the occurrence of different slope stability problems. Almost all these problems are related with structurally controlled failures and these are clearly observed in the roads and highways. The methodology used in this investigation is not the best for that kind of analysis. A kinematic analysis and proposing failure mechanisms such as plane failure, or wedge failure may be the most representative for studying that problems.

The precipitation scenario by itself produce the bigger displacements in the slope, however, the stability of the slope is not affected by this displacements. This situation could be grounded that materials tends to behave more plastic in saturated conditions and the permissible displacements increase.

Related with the different scenarios included in this investigations, the combination between dynamic + precipitation is the most representative of the failure occurrence. Another theory may be related with the active fault system E-W. A considerable seismic event ($K_{x,y}>0.50g$) may active a near fault (San Agustin Fault) and provoke a considerable displacements that overcome the maximum permissible displacements of the slope.

The creation of the different scenarios in any slope stability analysis is long dependence on the feasibility of data acquisition. The knowledge of all the characteristics (e.g. geology, seismicity, precipitation, physical-mechanical properties) will help to have a

better conceptual model and a more deterministic analysis. This work is based on a compilation of data from different sources in order to achieve the more possible deterministic analysis.

7. Conclusions

The tectonical location of the study zone has been characterized by the occurrence of different slope instability phenomena. This stability problems may be observed in a small scale such as road cuts or in bigger scales such as natural slopes or volcano flank collapses. The presence of an active fault system (e.g. MAFS) in combination with the environment conditions (precipitations) and the poor geomechanical characteristics of materials makes the zone an important study zone for the slope instability analysis in different scales. Next, the most remarkable conclusion are listed:

- Methodology proposed has been efficient for the procurance of all the data. It includes the laboratory tests, the use of empirical equations for the determination of the mechanical parameters and the software implemented have proven works perfectly with this study.
- Observations on fieldwork shows a remarkable variation between geological units. The zone is mainly conformed by pyroclastic products and lava flows deposits. The poor values of GSI suggest are due the high fracturing of welded units or by the brittle characteristics of poor welded ignimbrites.
- The GHB was the best option for the attribution of mechanical properties to rock masses. It is the only criterion which fits perfectly for the analyses of rock slopes and it has the advantage of proposed a non-linear mechanical behavior of rock masses.
- Seismic data used in this investigation for the determination of the maximum ground accelerations were convincing since they were obtained precisely in the study zone. On the other hand, precipitation data are realistic as long as there are more than forth meteorological station that are constantly registering precipitation data.
- The four proposed scenarios for the calculus of the displacements and FOS were adequate. The consideration of and earthquake and pouring rain may be the most representative trigger factors in the zone. The FEM and LEM thorw similar results for each scenario.

- The slope present condition of stability (FOS>1) in almost all the scenarios for LEM and FEM. However, the seismic acceleration has more influence on the stability. This situation is demonstrate in the analysis were seismic acceleration were incremented into 0.30g and 0.45 g. The precipitation analysis has the bigger displacements but the FOS>1. This situation indicates a plastic behavior of the sliding mass.

8. Technical considerations and future studies

It is very important to realize more laboratory tests on intact rock, tri-axial test may help for the determination of the principal stresses on the rock mass. Also, transmission of seismic waves for the determination of the dynamic modulus of materials may help.

Due the importance of the study zone, this investigation may be complemented with a smaller scale analysis such as a kinematic analysis.

Indirect methods may also complement this type of investigation as well as studies of the soil and another loads that were not considered in this investigation.

For future studies, seismic acceleration may be proposed as the main trigger factor in the zone. Otherwise, special attention may be put in the filling material of discontinuities, if the material is plastic clay, during rainy season this material will increase their volume creating normal stresses that may provoke a failure.

Bibliography

Acocella, V., & Puglisi, G. (2013). How to cope with volcano flank dynamics? A conceptual model behind possible scenarios for Mt. Etna. *Journal of Volcanology and Geothermal Research*, *251*, 137–148. https://doi.org/10.1016/j.jvolgeores.2012.06.016

Agliardi, F., & Crosta, G. B. (2003). High resolution three-dimensional numerical modelling of rockfalls. *International Journal of Rock Mechanics and Mining Sciences*, *40*(4), 455–471. https://doi.org/10.1016/S1365-1609(03)00021-2

Agliardi, F., Crosta, G., & Zanchi, A. (2001). Structural constraints on deep-seated slope deformation kinematics. *Engineering Geology*, *59*(1–2), 83–102. https://doi.org/10.1016/S0013-7952(00)00066-1

Barton, N., Lien, R., & Lunde, J. (1974). Engineering classification of rock masses for the design of tunnel support. *Rock Mechanics Felsmechanik Mécanique Des Roches*, *6*(4), 189–236. https://doi.org/10.1007/BF01239496

Basahel, H., & Mitri, H. (2017). Application of rock mass classification systems to rock slope stability assessment: A case study. *Journal of Rock Mechanics and Geotechnical Engineering*, *9*(6), 993–1009. https://doi.org/10.1016/j.jrmge.2017.07.007

Bieniawski, Z. T. (1973). Engineering Classification of Jointed Rock Masses. *Civil Engineer in South Africa*, *15*(12), 343–353. https://doi.org/http://dx.doi.org/10.1016/0148-9062(74)92075-0

Bieniawski, Z. T. (1974). *Geomechanics classification of rock masses and its application in tunneling*. *[No source information available]* (Vol. 2).

Bieniawski, Z. T. (1979). The geomechanics classification in rock engineering applications. *Proceedings of the 4th International Congress on Rock Mechanics*, 41–48.

Bieniawski, Z. T. (1993). 22 – Classification of Rock Masses for Engineering: The RMR System and Future Trends. In *Rock Testing and Site Characterization* (pp. 553–573). https://doi.org/10.1016/B978-0-08-042066-0.50028-8

Blatter, D. L., & Hammersley, L. (2010). Impact of the Orozco Fracture Zone on the central Mexican Volcanic Belt. *Journal of Volcanology and Geothermal Research*, *197*(1–4), 67–84. https://doi.org/10.1016/j.jvolgeores.2009.08.002

Blyth, F. G. H., & Freitas, M. H. (1984). A Geology for Engineers. *Nature*, *153*(3886), 476–477. https://doi.org/10.1038/153476b0

Borselli, L., Capra, L., Sarocchi, D., & De la Cruz-Reyna, S. (2011). Flank collapse scenarios at Volcán de Colima, Mexico: A relative instability analysis. *Journal of Volcanology and Geothermal Research*, *208*(1–2), 51–65. https://doi.org/10.1016/j.jvolgeores.2011.08.004

Brideau, M. A., Yan, M., & Stead, D. (2009). The role of tectonic damage and brittle rock fracture in the development of large rock slope failures. *Geomorphology*, *103*(1), 30–49. https://doi.org/10.1016/j.geomorph.2008.04.010

Brown, E. T. (2008). Estimating the mechanical properties of rock masses. *1st Southern Hemisphere International Rock Mechanics Symposium*, 3–22.

Canadian Geotechnical Society. (1985). Canadian Foundation Engineering Manual. *Canadian Foundation Engineering Manual*, *4*, 143–149.

Cantagrel, J. M., & Robin, C. (1979). K-Ar dating on eastern Mexican volcanic rocks - Relations between the andesitic and the alkaline provinces. *Journal of Volcanology and Geothermal Research*, *5*(1–2), 99–114. https://doi.org/10.1016/0377-0273(79)90035-0

Colunga, A. T., & Mena, E. (2015). Diseño De Obras Civiles De Cfe, (1).

Crombie Howe, R. (1997). *Geologic Contacts*. *Journal of Geoscience Education* (Vol. 45). https://doi.org/10.5408/1089-9995-45.2.133

Dobson, P., Gasperikova, E., Spycher, N., Lindsey, N. J., Guo, T. R., Chen, W. S., … Fowler, A. P. G. (2018). Conceptual model of the Tatun geothermal system, Taiwan. *Geothermics*, (June 2017), 0–1. https://doi.org/10.1016/j.geothermics.2018.01.001

Eberhardt, E., Stead, D., & Coggan, J. S. (2004). Numerical analysis of initiation and progressive failure in natural rock slopes-the 1991 Randa rockslide. *International Journal of Rock Mechanics and Mining Sciences*, *41*(1), 69–87. https://doi.org/10.1016/S1365-1609(03)00076-5

Edelbro, C. (2003). Rock mass strength: a review. *Technical Report; Department of Civil Engineering, Division of Rock Mechanics*, *16*, 1402–1536.

Ego, F., & Ansan, V. (2002). Why is the Central Trans-Mexican Volcanic Belt (102°-99°W) in transtensive deformation? *Tectonophysics*, *359*(1–2), 189–208. https://doi.org/10.1016/S0040-1951(02)00511-5

ESRI. (2016). ArcMap 10.3. *ESRI, Redlands, California.* Retrieved from http://resources.arcgis.com/en/help/main/10.2/index.html#/What_is_a_geoprocessing_service/0154000004v5000000/

Ferrari, L., Conticelli, S., Vaggelli, G., Petrone, C. M., & Manetti, P. (2000). Late Miocene volcanism and intra-arc tectonics during the early development of the Trans-Mexican Volcanic Belt. *Tectonophysics*, *318*(1–4), 161–185. https://doi.org/10.1016/S0040-1951(99)00310-8

Ferrari, L., López-Martínez, M., & Rosas-Elguera, J. (2002). Ignimbrite flare-up and deformation in the southern Sierra Madre Occidental, western Mexico: Implications for the late subduction history of the Farallon plate. *Tectonics*, *21*(4), 1–25. https://doi.org/10.1029/2001TC001302

Ferrari, L., Orozco-Esquivel, T., Manea, V., & Manea, M. (2012). The dynamic history of the Trans-Mexican Volcanic Belt and the Mexico subduction zone. *Tectonophysics*, *522–523*, 122–149. https://doi.org/10.1016/j.tecto.2011.09.018

Ferrari, L., Pasquare, G., & Tibaldi, A. (1990). Plio-Quaternary tectonics of the central Mexican Volcanic Belt and some constraints on its rifting mode. *Geofisica Internacional*.

Fowler, A. P. G., Ferguson, C., Cantwell, C. A., Zierenberg, R. A., McClain, J., Spycher, N., & Dobson, P. (2018). A conceptual geochemical model of the geothermal system at Surprise Valley, CA. *Journal of Volcanology and Geothermal Research*, *353*, 132–148. https://doi.org/10.1016/j.jvolgeores.2018.01.019

Garduño-Monroy, V. H., Arreygue-Rocha, E., Israde-Alcántara, I., & Rodríguez-Torres, G. M. (2001). Efectos de las fallas asociadas a sobreexplotaci??n de acu??feros y la presencia de fallas potencialmente s??smicas en Morelia, Michoac??n, M??xico. *Revista Mexicana de Ciencias Geologicas*, *18*(1), 37–54.

Garduño-Monroy, V. H., Pérez-Lopez, R., Israde-Alcantara, I., Rodríguez-Pascua, M. A., Szynkaruk, E., Hernández-Madrigal, V. M., … Mora Chaparro, J. C. (2009). Paleoseismology of the southwestern Morelia-Acambay fault system, central Mexico. *Geofisica Internacional*, *48*(3), 319–335.

Gómez-Vasconcelos, M. G., Garduño-Monroy, V. H., Macías, J. L., Layer, P. W., & Benowitz, J. A. (2015). The Sierra de Mil Cumbres, Michoacán, México: Transitional volcanism between the Sierra Madre Occidental and the Trans-Mexican Volcanic Belt. *Journal of Volcanology and Geothermal Research*, *301*, 128–147. https://doi.org/10.1016/j.jvolgeores.2015.05.005

González-Garcia, J., & Jessell, M. (2016). A 3D geological model for the Ruiz-Tolima Volcanic Massif (Colombia): Assessment of geological uncertainty using a stochastic approach based on Bézier curve design. *Tectonophysics*, *687*, 139–157. https://doi.org/10.1016/j.tecto.2016.09.011

Guilbaud, M. N., Siebe, C., Layer, P., & Salinas, S. (2012). Reconstruction of the volcanic history of the Tacámbaro-Puruarán area (Michoacán, México) reveals high frequency of Holocene monogenetic eruptions. *Bulletin of Volcanology*, *74*(5), 1187–1211. https://doi.org/10.1007/s00445-012-0594-0

Guilbaud, M. N., Siebe, C., Layer, P., Salinas, S., Castro-Govea, R., Garduño-Monroy, V. H., & Le Corvec, N. (2011). Geology, geochronology, and tectonic setting of the Jorullo Volcano region, Michoacán, México. *Journal of Volcanology and Geothermal Research*, *201*(1–4), 97–112. https://doi.org/10.1016/j.jvolgeores.2010.09.005

Hammah, R., Yacoub, T., & Corkum, B. (2008). The practical modelling of discontinuous rock masses with finite element analysis. *42nd US Rock Mechanics Symposium and 2nd U.S. - Canada Rock Mechanics Symposium*, (January), 56–63. Retrieved from https://www.rocscience.com/assets/files/uploads/7704.pdf

Hasenaka, T., & Carmichael, I. S. E. (1985). The cinder cones of Michoac??n-Guanajuato, central Mexico: their age, volume and distribution, and magma discharge rate. *Journal of Volcanology and Geothermal Research*, *25*(1–2), 105–124. https://doi.org/10.1016/0377-0273(85)90007-1

Hills, E. S. (1972). *Elements of Structural Geology* (2nd ed.). London. https://doi.org/10.1007/978-94-009-5843-2

Hinojosa-Corona, A., Rodríguez-Moreno, V. M., Munguía-Orozco, L., & Meillón-Menchaca, O. (2011). El deslizamiento de ladera de noviembre 2007 y generación de

una presa natural en el río Grijalva, Chiapas, México. *Boletin de La Sociedad Geologica Mexicana*, *63*(1), 15–38.

Hobbs, B. E., Means, W. D., & Williams, P. F. (1976). *An Outline of Structural Geology*. Wiley. Retrieved from https://books.google.com.mx/books?id=XJGNQgAACAAJ

Hoek, E. (1983). Strength of jointed rock masses. *Geotechnique*, *23*(3), 187–223. https://doi.org/10.1680/geot.1983.33.3.187

Hoek, E., Carranza, C., & Corkum, B. (2002). Hoek-brown failure criterion – 2002 edition. *Narms-Tac*, 267–273. https://doi.org/10.1016/0148-9062(74)91782-3

Hoek, E., Marinos, P., & Benissi, M. (1998). Applicability of the geological strength index (GSI) classification for very weak and sheared rock masses. The case of the Athens Schist Formation. *Bulletin of Engineering Geology and the Environment*, *57*(2), 151–160. https://doi.org/10.1007/s100640050031

Hoek, E., Marinos, P. G., & Marinos, V. P. (2005). Characterization and engineering properties of tectonically undisturbed but lithologically varied sedimentary rock masses. *International Journal of Rock Mechanics and Mining Sciences*, *42*(2), 277–285. https://doi.org/10.1016/j.ijrmms.2004.09.015

Housner, G. W. (1970) "Strong ground motion en Earthquake engineering", R. Wiegel, editor, Prentice-Hall, Englewood Cliffs, New Jersey.

ISRM. (1978). The Complete ISRM Suggested Methods for Rock Characterization, Testing and Monitoring; 1974-2006. *Environmental and Engineering Geoscience*, *15*(1), 47–48. https://doi.org/10.2113/gseegeosci.15.1.47

Kahraman, S. (2014). The determination of uniaxial compressive strength from point load strength for pyroclastic rocks. *Engineering Geology*, *170*, 33–42. https://doi.org/10.1016/j.enggeo.2013.12.009

Kramer S.L., (1996) "Geotechnical earthquake engineering". Prentice Hall. New Yersey, 653 p.

Kshirsagar, P., Siebe, C., Guilbaud, M. N., & Salinas, S. (2016). Geological and environmental controls on the change of eruptive style (phreatomagmatic to Strombolian-effusive) of Late Pleistocene El Caracol tuff cone and its comparison with adjacent volcanoes around the Zacapu basin (Michoacán, México). *Journal of Volcanology and Geothermal Research*, *318*, 114–133. https://doi.org/10.1016/j.jvolgeores.2016.03.015

Kshirsagar, P., Siebe, C., Guilbaud, M. N., Salinas, S., & Layer, P. W. (2015). Late Pleistocene Alberca de Guadalupe maar volcano (Zacapu basin, Michoacán): Stratigraphy, tectonic setting, and paleo-hydrogeological environment. *Journal of Volcanology and Geothermal Research*, *304*, 214–236. https://doi.org/10.1016/j.jvolgeores.2015.09.003

Makdisi F.I., Seed H.B., (1978), "Simplified procedure for computing maximum acceleration and natural period for embankments". Report UCB/EERC-77/19, Eartquake engineering research center, University of California, Berkeley, California.

Marinos, P., & Hoek, E. (2001). Estimating the geotechnical properties of heterogeneous rock masses such as flysch. *Bulletin of Engineering Geology and the Environment*, *60*(2), 85–92. https://doi.org/10.1007/s100640000090

Marinos, V., Marinos, P., & Hoek, E. (2007). Geological Strength Index (GSI). A characterization tool for assessing engineering properties for rock masses. *Underground Works under Special Conditions*, (July), 13–21. https://doi.org/10.1201/NOE0415450287.ch2

Martínez-Reyes, J., & Nieto-Samaniego, A. F. (1990). Efectos geológicos de la tectónica reciente en la parte central de México. *Universidad Nacional Autónoma de México, Revista Del Instituto de Geología*, *9*, 33–50.

Martini, M., Ferrari, L., Lopez-Martinez, M., Cerca-Martinez, M., Valencia, V. a, & Serrano-Duran, L. (2009). Cretaceous-Eocene magmatism and Laramide deformation in southwestern Mexico: No role for terrane accretion. *Geological Society of America Memoirs*, *204*(07), 151–182. https://doi.org/10.1130/2009.1204(07).

Martini, M., Ferrari, L., López-martínez, M., & Valencia, V. (2010). Stratigraphic redefinition of the Zihuatanejo area , southwestern Mexico. *Revista Mexicana de Ciencias Geológicas*, *27*(3), 412–430.

Morán-Zenteno, D. J., Corona-Chavez, P., & Tolson, G. (1996). Uplift and subduction erosion in southwestern Mexico since the Oligocene: pluton geobarometry constraints. *Earth and Planetary Science Letters*, *141*(1–4), 51–65. https://doi.org/10.1016/0012-821X(96)00067-2

Nelson, E. P., Connors, K. A., & Suárez S., C. (2007). GIS-based slope stability analysis, Chuquicamata open pit Copper Mine, Chile. *Natural Resources Research*. https://doi.org/10.1007/s11053-007-9044-7

Nieto O, J., Delgado A, L., & Damon, P. E. (1985). Geochronologic, petrologic, and structural data related to large morphologic features between the Sierra Madre Occidental and the mexican volcanic belt. *Geof. Int*, *24–4*, 623–663. Retrieved from http://www.revistas.unam.mx/index.php/geofisica/article/view/39814/36231

Orozco-Esquivel, M. T., Ferrari, L., & López-Martínez, M. (2009). La Sierra de Mil Cumbres: Geocronología y geoquímica del volcanismo inicial de la Faja Volcánica Transmexicana. *Geosphere*, *29*(1), 70.

OROZCO-ESQUIVEL, T., LÓPEZ-MARTÍNEZ, M., LONSDALE, P., FERRARI, L., CORNEJO-JIMENEZ, C., PINERO-LAJAS, D., & DUQUE-TRUJILLO, J. F. (2010). Tearing apart of an early Miocene silicic igneous province in the southern Gulf of California. In *2010 GSA Denver Annual Meeting*.

Ortega-Rivera, A. (2003). Geochronological constraints on the tectonic history of the Peninsular Ranges Batholith of Alta and Baja California: Tectonic implications for western México. In S. E. Johnson, S. R. Paterson, J. M. Fletcher, G. H. Girty, D. L. Kimbrough, & A. Martín-Barajas (Eds.), *Tectonic evolution of northwestern Mexico and the Southwestern USA*. Geological Society of America. Retrieved from http://dx.doi.org/10.1130/0-8137-2374-4.297

Palmström, A. (2001). Measurement and characterizations of rock mass jointing. *In-Situ Characterization of Rocks - Chapter 2*, 1–40.

Pardo, M., & Suárez, G. (1995). Shape of the subducted Rivera and Cocos plates in southern Mexico: Seismic and tectonic implications. *Journal of Geophysical Research*, *100*(B7), 12357. https://doi.org/10.1029/95JB00919

Park, H.-J., Lee, J.-H., Kim, K.-M., & Um, J.-G. (2016). Assessment of rock slope stability using GIS-based probabilistic kinematic analysis. *Engineering Geology*, *203*, 56–69. https://doi.org/10.1016/j.enggeo.2015.08.021

Pasquarè, G., Ferrari, L., Garduño-Monroy, V. H., Tibaldi, A., & Vezzoli, L. (1991). Geology of the central sector of the Mexican Volcanic belt, States of Guanajuato and Michoacán. *Geological Society of America Map and Chart Series MCH072*, (JANUARY), 22 p.

Pedrazzini, A., Jaboyedoff, M., Loye, A., & Derron, M. H. (2013). From deep seated slope deformation to rock avalanche: Destabilization and transportation models of the Sierre landslide (Switzerland). *Tectonophysics*, *605*, 149–168. https://doi.org/10.1016/j.tecto.2013.04.016

Pola, A., Martínez-Martínez, J., Macías, J. L., Fusi, N., Crosta, G., Garduño-Monroy, V. H., & Núñez-Hurtado, J. A. (2016). Geomechanical characterization of the Miocene Cuitzeo ignimbrites, Michoacán, Central Mexico. *Engineering Geology*, *214*, 79–93. https://doi.org/10.1016/j.enggeo.2016.10.003

Potgieter, J. (2016). Finite Element Versus Limit Equilibrium Stability Analyses for Surface Excavations.

Price, N. J. (2016). *Fault and joint development: in brittle and semi-brittle rock*. Elsevier.

Priest, S. (1993). *Discontinuity Analysis for Rock Engineering*. *Journal of Chemical Information and Modeling* (Vol. 53). https://doi.org/10.1017/CBO9781107415324.004

Qi, C., Wu, J., Liu, J., & Kanungo, D. P. (2016). Assessment of complex rock slope stability at Xiari, southwestern China. *Bulletin of Engineering Geology and the Environment*. https://doi.org/10.1007/s10064-015-0763-4

Ritter, W. (1879). Die statik der tunnelgewölbe. Berlin: J. Springer. Retrieved from file://catalog.hathitrust.org/Record/100780102

Robinson, S., Brooks, R., & Kotiadis, K. (2011). *Conceptual Modeling for Discrete-Event Simulation*. *Annals of Operations Research*.

Romaña, J. (2014). *Los Limites de la Ley de Darcy*. *Bdigital.Unal.Edu.Co*. Universidad Nacional de Colombia.

Schön, J. H. (2015). Physical Properties of Rocks: Fundamentals and Principles of Petrophysics (2nd edition). *Developments in Petroleum Science (Elsevier)*, *65*, 499. https://doi.org/10.1017/CBO9781107415324.004

Seed, H.B. (1970) “Soil problems and Soil behavior, Earthqueake Engineering, R.L”. Wiegel Ed. Englewood Cliffs, New Jersey: Prentice-Hall, Chapter 10.

Styles, T., Daniel, T., & Hons, S. (2015). Numerical Modelling and Analysis of slope stability within fracture dominated rock masses Numerical Modelling and Analysis of slope stability within fracture dominated rock masses, (January 2009). https://doi.org/10.13140/RG.2.1.4225.0969

Suárez González, A. (2014). *Estudio del potencial de almacenamiento de CO2 en rocas de facies Cretáciocas de la formación Boñar a partir de ensayos de densidad, porosidad y permeabilidad*. Universidad de León.

Suarez, J. (1978). Capítulo 7 Comportamiento Sísmico de los Taludes. *Deslizamientos: Análisis Geotecnico*.

Suter, M., Martínez, M. L., Legorreta, O. Q., & Martínez, M. C. (2001). Quaternary intra-arc extension in the Central Trans-Mexican volcanic belt. *Bulletin of the Geological Society of America*, *113*(6), 693–703. https://doi.org/10.1130/0016-7606(2001)113<0693:QIAEIT>2.0.CO;2

Szynkaruk, E., Graduno-Monroy, V. H., & Bocco, G. (2004). Active fault systems and tectono-topographic configuration of the central Trans-Mexican Volcanic Belt. *Geomorphology*, *61*(1–2), 111–126. https://doi.org/10.1016/j.geomorph.2003.10.006

Taylor & Francis Group. (2011). *Conceptual Modeling for Discrete-Event Simulation*. (R. (University of L. Brooks, S. (University of W. Robinson, & K. (University of W. Kotiadis, Eds.), *Annals of Operations Research*. Boca Raton, FL.

Tiab, D., & Donaldson, E. C. (2015). *Petrophysics: Theory and Practice of Measuring Reservoir Rock and Fluid Transport Properties: Fourth Edition*. *Petrophysics: Theory and Practice of Measuring Reservoir Rock and Fluid Transport Properties: Fourth Edition*. https://doi.org/10.1016/C2014-0-03707-0

Verma, S. P., López-Martínez, M., & Terrell, D. J. (1985). Geochemistry of Tertiary igneous rock from Arandas–Atotonilco area, north- east Jalisco, Mexico. *Geof. Int.*, *24–1*, 31–45. Retrieved from http://www.revistas.unam.mx/index.php/geofisica/article/view/39306/35745

Yang, T., Grand, S. P., Wilson, D., Guzman-Speziale, M., Gomez-Gonzalez, J. M., Dominguez-Reyes, T., & Ni, J. (2009). Seismic structure beneath the Rivera subduction zone from finite-frequency seismic tomography. *Journal of Geophysical Research: Solid Earth*, *114*(1). https://doi.org/10.1029/2008JB005830

Zhang, L. (2006). Engineering Properties of Rocks. *Elsevier Geo-Engineering Book Series*, *Volume 4*, 1–290. https://doi.org/10.1016/S1571-9960(06)80006-6